CHAPTER 12

# *Differentiation of Magmas*

## Fundamental Questions Considered in This Chapter

1. Once magma has been generated in the lower crust or upper mantle, how can its composition be modified by subsequent differentiation processes?
2. What petrologic tools are available to unravel the effects of multiple processes that are involved in the origin and evolution of magmas?

## INTRODUCTION

The origin of the broad compositional spectrum of magmatic rocks (e.g., Figure 2.4) has been one of the most fundamental problems in igneous petrology. In the previous chapter, it was demonstrated that variable source compositions and conditions allow generation of diverse primary magmas, but these fall short of accounting for the entire spectrum. Further modification of diverse primary magmas results from the overprinting effects of magmatic differentiation on primary magmas after leaving their source.

Near the surface of the Earth, rocks solidifying from undifferentiated, unmodified primary magmas are the exception rather than the rule. For example, most basaltic lavas have compositions that are not in equilibrium with their mantle peridotite source because olivine fractionation—one form of magmatic differentiation—takes place in the magma en route to the surface. Intrusions of basaltic magma that internally differentiate into layers of olivine (dunite rock), pyroxene (pyroxenite), and plagioclase (anorthosite) provide examples of the modifications that can happen.

The compositions of primary magmas ascending buoyantly out of mantle and deep crustal sources are modified to varying degrees by several processes of **differentiation.** Insights into this overprint can be gleaned from study of a suite of compositionally variable rocks that are closely related or associated in space and time: That is, they occur within a restricted geographic area and are of about the same age. Examples include rocks within a layered basaltic intrusion or a Hawaiian shield volcano. A necessary condition for a genetic relation between rocks and the magmas from which they solidified is that they are so related, but this is not sufficient to guarantee a **comagmatic,** or **cogenetic,** kinship via differentiation. Magmas from different sources or at least different evolving batches might, coincidentally, make up a composite intrusion or a long-lived composite volcano. Usually, a petrologist hypothesizes that a suite of rocks related in space and time are comagmatic, on the basis of some form of preliminary evidence, such as field relations and petrographic attributes. Additional chemical, isotopic, mineralogical, and modal compositions; trends in composition; precise isotopic dating; and other information can then be used to test for kinship. From these laboratory data, a **parent magma** is hypothesized; from it the more evolved rocks of the suite are assumed to have been derived by differentiation processes to be determined. A parent magma is usually not primary, or wholly unmodified from its source, but is at least primitive, having been modified less than other magmas that formed the comagmatic suite (Section 11.3.5). In many instances, an unseen parent must be hypothesized.

Differentiation processes can be outlined as follows:

I. Closed-system processes
   A. Crystal-melt fractionation
      1. Gravitational segregation

2. Flowage segregation
3. Filter pressing
4. Convective melt fractionation

B. Physical separation of immiscible melts
C. Melt-fluid separation

II. Open-system processes
A. Assimilation of an initially solid contaminant
B. Mixing of two or more contrasting magmas

Two or more of these processes commonly operate simultaneously or in tandem. For example, magma in a continental arc chamber may evolve from some primitive parent by crystal-melt fractionation while assimilating wall rock; this daughter magma may subsequently mix with another magma.

The plan of this chapter is first to present the basic principles of differentiation illustrated with simple examples, then to describe rock associations formed by more complex compound processes.

## ✲12.1 USING VARIATION DIAGRAMS TO CHARACTERIZE DIFFERENTIATION PROCESSES

Chemical variation diagrams that show coherent, regular compositional trends in a suite of comagmatic rocks can provide information on differentiation processes (Cox et al., 1979). Changing melt compositions (liquid lines of descent, e.g., Figures 5.23b and 8.16) during crystal-melt fractionation and proportions of two mixed magmas and amount of a solid contaminant can be determined. Graphical modeling techniques presented here, mostly for cartesian diagrams of two variables (*x*-*y* plots), can be readily adapted to a personal computer using widely available spreadsheet software.

Thorough sampling of fresh (unaltered) representative rocks and accurate laboratory analysis (Section 2.1) are crucially important in graphical modeling. So too is a careful petrographic study, as this is one means by which working hypotheses are formulated and tested by variation diagrams in which element concentrations and isotopic ratios are plotted. One diagram violating a hypothesis is sufficient to invalidate it, or possibly to indicate it needs some modification. For example, modification of the composition of the assumed, unseen parent magma may be required. Complete agreement with available data only indicates that the hypothesis hasn't been disproved.

Compositional patterns of suites of unaltered volcanic rocks are generally more amenable to unambiguous interpretation than plutonic rocks that might have suffered inconspicuous subsolidus modifications during slow cooling. Although the inverse procedure of inferring process from product always has some degree of ambiguity and uncertainty, volcanic suites may closely represent extruded melts that evolved along liquid lines of descent. Volcanic rocks provide the opportunity to compare compositions of coexisting crystals and melt, represented in phenocrysts and surrounding glassy or aphanitic groundmass, respectively.

If some mass *A* is *added* to magma *B* in Figure 12.1, in which their compositions are represented by constituents *x* and *y,* the resultant hybrids plot along a straight line *AB.* Constituents *x* and *y* can be major elements or their oxides (in weight percentage) or trace elements (in parts per million); the latter generally have a greater range of variation within a comagmatic rock suite and serve as reliable indicators of differentiation processes. For a particular combination of *A* and *B,* say, *C,* the proportions of the two end members are given by the lever rule (equation 5.2). The mass of added *A* could be an assimilated contaminant into magma *B,* or *A* and *B* could be two mixed magmas, or *B* might be a parent magma from which precipitating crystals of uniform composition *A* accumulate a fixed amount by some means, forming a cumulate *C.* In the case in which *A* is *subtracted* from *B* a residue *R* is created. *B* might be a parent magma from which uniform crystals of *A* are fractionated out. The linear trends on this two-element variation diagram do not apply where *x* or *y* is a ratio of elements. Figure 12.2a–c shows two-element variation diagrams for a system in which more than one phase of fixed composition is fractionated from a parent magma.

Linear (straight line) trends on two-element diagrams are typically found in rock suites produced by mixing of two magmas and by assimilation of foreign rock into a magma because combinations of two compositionally fixed end members are involved. Additional information can indicate which of these two common possible differentiation processes operated.

Fractionating a solid solution of variable composition is a typical process in a crystallizing parent magma and yields a nonlinear (curved) trend in residual melts (Figure 12.2d).

Compositional trends for three constituents can be represented on ternary diagrams, but these provide no absolute concentration values.

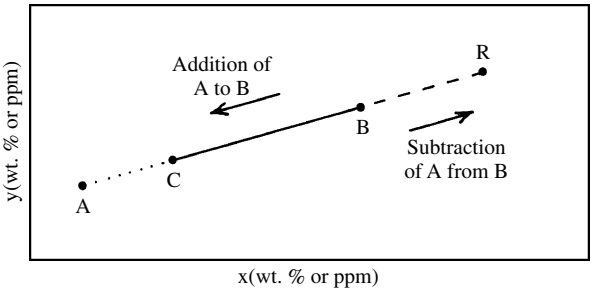


**12.1** Hypothetical two-element variation diagram. The line *ACBR* is a **control line.**

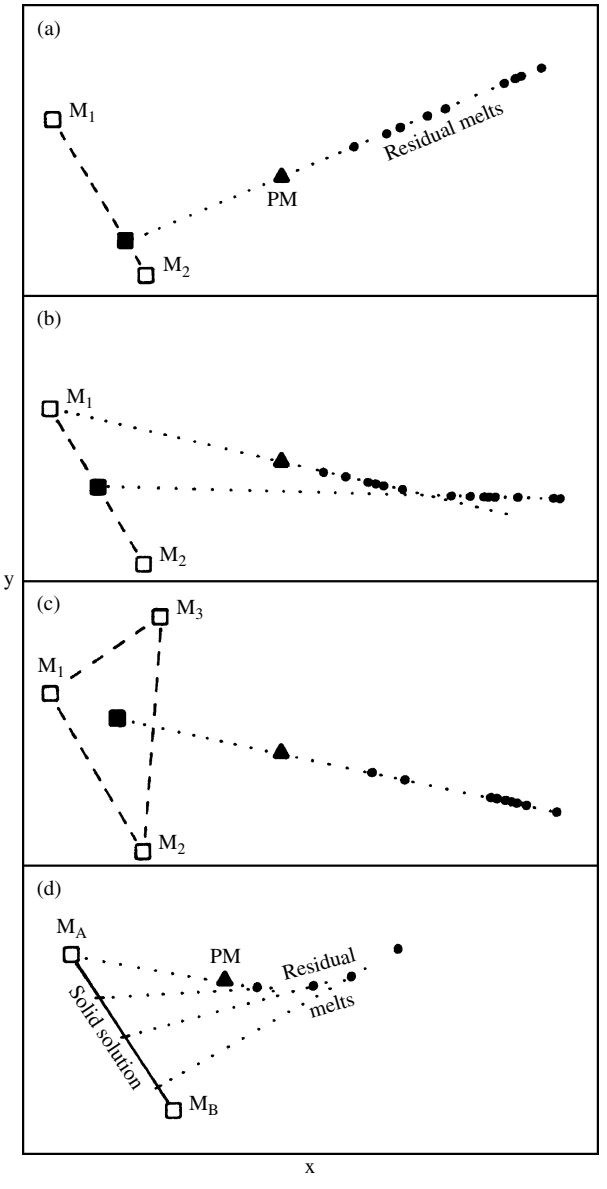


**12.2** More complex two-element variation diagrams and **control lines** (dotted). (a) Two minerals, $M_1$ and $M_2$, in the proportions of 80:20 fractionate in varying amounts from a parent magma, PM, to produce variable residual evolved daughter melts (filled circles). (b) Mineral $M_1$ fractionates alone followed by cofractionation of equal proportions of $M_1$ and $M_2$. (c) Three minerals, $M_1$, $M_2$, and $M_3$, cofractionate in equal proportions from the parent magma. (d) Solid solutions between end members $M_A$ and $M_B$ fractionate successively, producing a curved residual melt trend; successive control lines are tangential to the curve at the intermediate "parent" melt that was produced as a residue of the previous fractionation.

## ❋12.2 CLOSED-SYSTEM MAGMATIC DIFFERENTIATION

With the recognition that magmas consist generally of melt plus crystals and locally an exsolved volatile fluid phase, three possible means of differentiation are logically possible in closed systems:

1. Separation of crystals and melt, called *crystal-melt fractionation, fractional crystallization,* or simply *fractionation*
2. Separation of two immiscible melts
3. Separation of melt and a fluid phase

### 12.2.1 Crystal-Melt Fractionation

**Crystal-melt fractionation** occupies a prominent status among all processes of magma differentiation and dominates in closed systems. Espoused as early as 1835 by Charles Darwin, fractionation was championed by Bowen (1928) through the first half of the 20th century (Young, 1998); Bowen referred to the process as *crystallization-differentiation* to emphasize that melt generally separates from growing crystals in dynamic magma systems.

Because of the contrast in chemical composition between any melt and its precipitating crystals, segregation of the two provides a powerful means of differentiating a parent magma into compositionally contrasting parts. For example, at 1020°C in the nearly crystallized Makaopuhi basalt magma (Plate III), a small proportion (about 10%) of silicic melt coexists with crystals of plagioclase, pyroxene, Fe-Ti oxides, and accessory apatite. Similar evolved melts that are enriched in silica, alkalies, and volatiles solidify to interstitial glass in many basalts (e.g., Table 12.1). Segregation of such a melt from the

**Table 12.1** Chemical and Normative Compositions of a Whole-Rock Basalt and a Small Percentage of Residual Glass Lying between Crystals, Holocene Santa Clara Lava Flow Near St. George, Utah[a]

| | BASALT | GLASS |
|---|---|---|
| $SiO_2$ | 51.1 | 66.5 |
| $TiO_2$ | 1.7 | 1.3 |
| $Al_2O_3$ | 14.3 | 13.9 |
| FeO | 10.4t | 1.9t |
| MgO | 8.1 | 0.1 |
| CaO | 9.2 | 0.9 |
| $Na_2O$ | 3.1 | 3.3 |
| $K_2O$ | 1.1 | 7.0 |
| Total | 99.0 | 94.9 |
| *Q* | 0.0 | 19.0 |
| *Or* | 6.5 | 41.2 |
| *Ab* | 26.2 | 27.7 |
| *An* | 21.5 | 2.4 |
| *Di* | 19.2 | 0.7 |
| *Hy* | 13.1 | 0.0 |
| *Ol* | 5.9 | 0.0 |
| *Mt* | 4.5 | 0.7 |
| *Il* | 3.2 | 2.4 |

[a] Note the low total for the glass that suggests about 5 wt.% volatiles, mainly water, in the microprobe analysis.

## Special Interest Box 12.1 Picrites erupted in 1959 from Kilauea volcano, Hawaii: Mixing, not olivine fractionation

An example of a two-oxide variation diagram with a linear pattern, like the simple model in Figure 12.1, is shown in Figure 12.3. This diagram shows compositions of basaltic lavas erupted from the summit of Kilauea volcano, Hawaii, in 1959. Note that all plotted oxides in the lavas fit linear olivine control lines; this finding is consistent with the hypothesis, presented in the first edition of this textbook, that the lavas were differentiated by addition and subtraction of compositionally uniform olivine phenocrysts to and from a parent magma. However, it is puzzling why the fractionated olivines would be so uniform in composition during what was probably extensive crystallization of the magma; a curved trend of differentiation would be expected for fractionation of changing solid solutions from a changing magma (Figures 12.2 and 12.5). Subsequent investigations of this unusual eruption and its lavas, summarized by Helz (1987), who also presents significant new data, have shown that the olivine fractionation hypothesis is faulty.

Examination of thin sections of the picrites reveals seven textural types of olivines, rather than a single simple population of phenocrysts. In addition to euhedral and skeletal crystals (likely phenocrysts) there are blocky crystals as much as 12 mm long that contain planar extinction discontinuities due to strain, anhedral grains that appear to be strongly resorbed, angular fragments(?), subhedral grains that contain sulfide inclusions, exceptionally large crystals (megacrysts as much as 20 mm in diameter), and metamorphic-textured aggregates. Most olivines regardless of textural type show evidence of partial resorption. Microprobe analyses reveal rather uniform compositions, $Fo_{84–89}$, but, in detail, indicate widespread disequilibrium in complex zoning.

Episodes of the November 14 to December 20, 1959, summit eruptions were unusual in recorded Hawaiian activity: Unusually extensive scoria deposits are of the most Mg-rich glass, erupted lavas were the hottest (1192°C), lava fountains were highest (580 m), and none of the summit lavas was also extruded on the flanks of the volcano, as commonly happens.

Altogether, the data suggest mixing of two magmas—a hot primitive, MgO-rich magma that ascended relatively rapidly from depths of 45–60 km in the mantle, passing through, and variably entraining a somewhat evolved magma stored in a subvolcanic chamber. In this model, texturally variable olivines represent crystallization products during decompression and cumulates in the crystallizing storage chamber. In addition, some mantle wall rock was assimilated into the ascending primitive magma.

This case history shows that although initial data can support a particular hypothesis (olivine fractionation), additional data can refute that hypothesis and a new one must be proposed (mixing of two magmas) to satisfy the whole body of information.

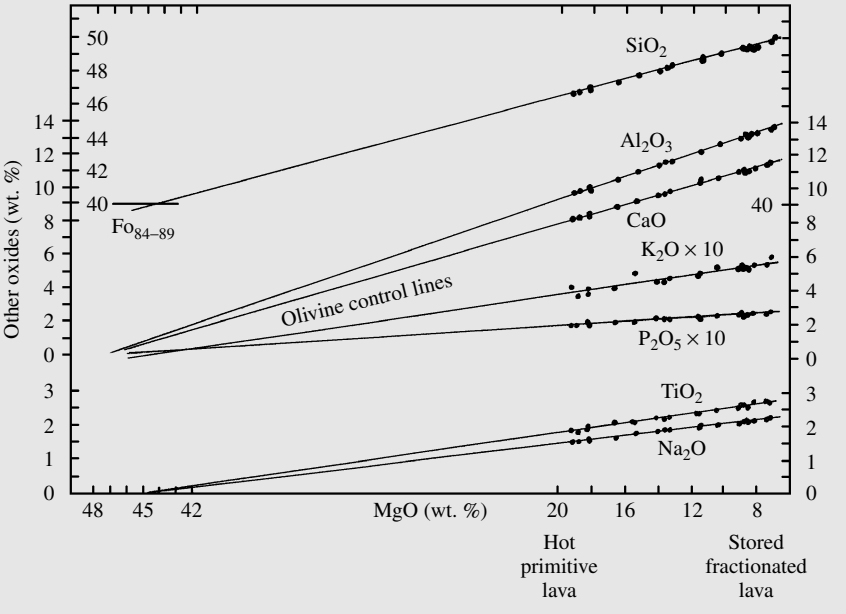


**12.3** Composite two-oxide variation diagram for lavas erupted from the summit of Kilauea volcano, Hawaii, in 1959. Each analyzed sample is plotted as a solid circle with respect to MgO on the horizontal axis against the weight percentage of other oxides on the vertical axis. Olivine control line drawn through MgO-$SiO_2$ analyses passes through the range of composition of analyzed olivines $Fo_{84–89}$ that have about 40 wt.% $SiO_2$ and 47–43 wt.% MgO (Helz, 1987). Other oxide control lines are near 0 wt.% at 47–43 wt.% MgO, reflecting their very small concentrations in the analyzed olivines. (Data from Murata and Richter, 1966.)

crystalline framework has been observed in some thick basalt flows and sills where it has collected into thin pods of granitic rock.

Thus, the effects of fractionation of a parent magma are manifested in complementary evolved residual melts and accumulated crystals. Rocks derived from residual melts have relatively evolved compositions and possibly phenocryst-free aphanitic or glassy texture.

Complementary accumulations of crystals that differ in composition not only from the separated melt but from the parent magma as well are called **cumulates.** Layers made virtually of only pyroxene, olivine, or plagioclase occur in some large, slowly cooled intrusions of basaltic magma. Such **monomineralic** layers of pyroxenite, dunite, or anorthosite, respectively, can only form by crystal accumulation because no magmas of equivalent composition are known to occur. Modest accumulation of a magnesian olivine near $Fo_{90}$ (Appendix A), such as typically crystallizes from primitive basalt magmas, enriches the magma in Mg but depletes the residual magma in Mg and enriches it in Si, Ti, Al, Ca, Na, K, and P. Summit extrusions of basaltic lavas from Kilauea volcano, Hawaii, in 1959 ranged from olivine-rich picrites to olivine-poor basalts. Picrite lavas carrying as much as 30% olivine were erupted at unusually high rates of discharge from the vent, creating exceptionally high (580 m) lava fountains. Analyses of these two extreme lavas show the anticipated variations in major elements (Table 12.2; Figure 12.3).

Trace Element Modeling of Fractional Crystallization. In evolving magmas, the effect of fractional crystallization is more obvious in trace element than major element variations. For example, fractional crystallization drives a subalkaline magma toward the composition of a minimum melt in the granite system (Figure 5.27a). In such high-$SiO_2$ granite magma, the coexisting melt and solids (subequal proportions of plagioclase, alkali feldspar, and quartz) have nearly the same major element composition, and large amounts of fractionation yield only small changes in major elements of, perhaps, 2 wt.% in $SiO_2$. However, trace element concentrations can vary by several hundred percent. (Interestingly, in some such rocks Mg qualifies as a trace element.) Powerful constraints on the crystal-melt fractionation can be provided by trace elements.

**Table 12.2** Compositions of Most Olivine-Rich Basalt (Picrite) and Most Olivine-Poor Basalt Erupted from the Summit of Kilauea Volcano, Hawaii, in 1959

| | Picrite | Olivine-Poor Basalt |
|---|---|---|
| $SiO_2$ | 46.93 | 49.89 |
| $TiO_2$ | 1.93 | 2.72 |
| $Al_2O_3$ | 9.77 | 13.46 |
| FeOt | 11.74 | 11.35 |
| MnO | 0.18 | 0.18 |
| MgO | 19.00 | 8.00 |
| CaO | 8.29 | 11.33 |
| $Na_2O$ | 1.58 | 2.25 |
| $K_2O$ | 0.39 | 0.55 |
| $P_2O_5$ | 0.19 | 0.27 |
| Total | 100.00 | 100.00 |

See also Figure 12.3.
(Data from Murata and Richter, 1966.)

During progressive crystallization of a magma, compatible elements are concentrated in the solids and incompatible elements are continuously enriched in the residual liquid. The extent of crystallization of a magma system is an important control on the trace element concentrations of the residual melt and the solids.

For a closed magma system undergoing perfect fractional crystallization, the relations among the bulk distribution coefficient, $D$ (Section 2.5.1); melt fraction, $F$; and concentration ratio of a particular element in the residual melt to that in the parent magma, $C_m/C_p$, are given by the Rayleigh law

$$\frac{C_m}{C_p} = F^{(D-1)} \qquad 12.1$$

This equation is plotted in Figure 12.4 for several values of $D$. The extent of fractional crystallization is especially critical for those elements that have either very high or very low bulk distribution coefficients. For a compatible element, such as Ni ($D_{Ni} \sim 7$), in a basaltic magma precipitating olivine ± pyroxene, the concentration of Ni in the residual melt decreases to 0.5 that in the parent magma after only 10% crystallization ($F = 0.1$) and to 0.01 after 54% crystallization. In contrast, the concentration of an incompatible element, such as Rb ($D_{Rb} \sim 0.001$), in the residual melt of the same parent magma has only doubled after 50% crystallization, and advanced crystallization, about 90%, is needed to increase its concentration in the residual melt 10-fold.

Incompatible element enrichment in residual melts can set the stage for subsequent processes to enrich them further, possibly into economic concentrations in ore deposits. Beryllium (Be) is an example. Be ore deposits are typically associated with highly evolved granites and rhyolites. In granite magma systems, melt-fluid separation can concentrate the Be into pegmatitic minerals (e.g., beryl) that can be mined (discussed later).

If distribution coefficients and fractionating crystalline phases are known or can be assumed with some degree of certainty, crystal-melt fractionation models can be compared with trends from analytical data on rock suites. A model for a fractionally crystallizing magma system in which melt and solid solutions are continuously varying is fitted to analytical data on a rock suite in Figure 12.5. The variation trend for compatible versus incompatible element is strongly curved.

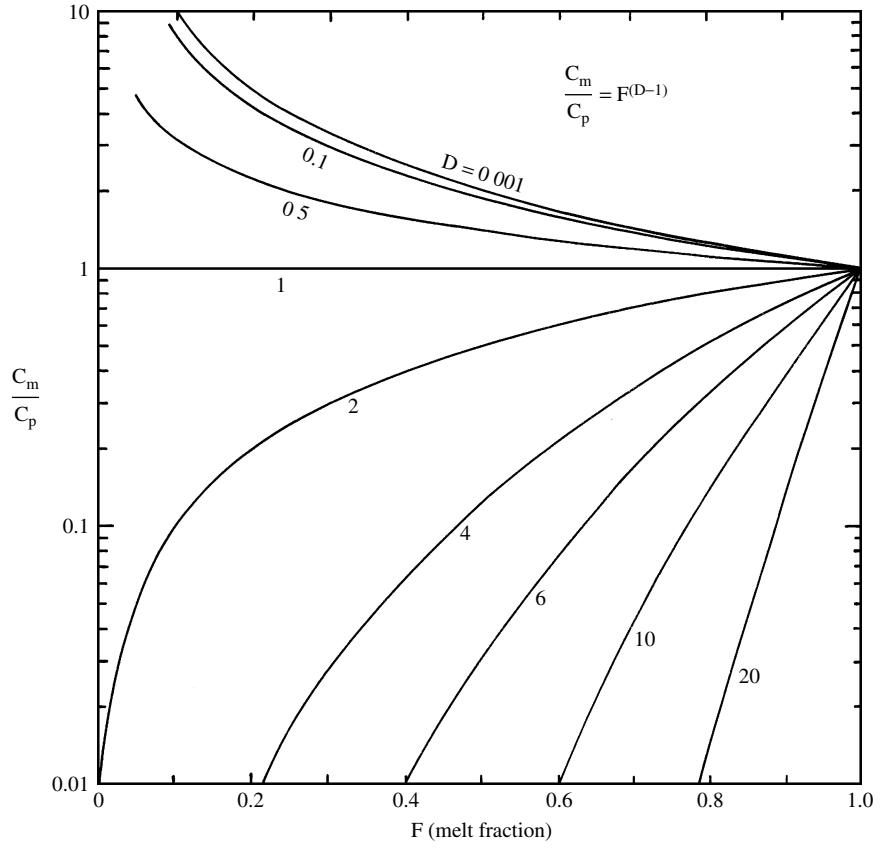


**12.4** Theoretical variation in concentration of an element in residual melts, $C_m$, formed by fractionation of crystals with a distribution coefficient, $D$, from an initial parent magma, $C_p$. See equation 12.1.

The trace element pattern of residual melts can reveal important information about what phases are fractionating (e.g., Table 2.6). For example, in silicic melts, depletion of compatible Eu and Sr results from plagioclase fractionation and of Ba from mica or K-feldspar fractionation.

Physical Mechanisms of Crystal-Melt Fractionation. Given the chemical efficacy of crystal-melt fractionation, how is it physically accomplished? Four mechanisms have been identified:

1. **Gravitational segregation.** In a static body of melt, denser crystals might sink whereas less dense ones might float. This process has been widely accepted as a viable means of crystal-melt fractionation. However, except for the hottest mafic melts and largest crystals, the plastic yield strength of melts (ignored in the formulation of Stokes's law, which assumes Newtonian viscosity, Section 8.3.3) may preclude much movement of isolated crystals. Further experimental studies of the role of yield strength in crystal movement are needed.
2. **Flowage segregation:** In moving bodies of magma, grain-dispersive pressure pushes crystals and other solid particles into the interior of the flowing magma away from conduit walls where there are strong velocity gradients (Figure 8.13). This phenomenon has been documented in many dikes (e.g., Figure 8.14), sills, and extrusions.
3. **Filter pressing:** A cloth or paper filter passes liquid through it but not suspended solid particles, which are trapped by the smaller openings in the filter. Residual melt in partially crystallized magmas can be filter pressed from the interlocking network of crystals because of local gradients in pressure. On the floor of a crystallizing magma chamber, the weight of accumulating crystals may press some of the entrapped residual melt out of the compacting crystal mush into the overlying magma. Movement of small interstitial volumes of usually evolved, viscous silicic melt entangled in a network of crystals (Plate III, 1020°C) and separation from the network would, intuitively, appear to be unlikely. However, during crystallization, the melt is commonly also enriched in water, thereby reducing its viscosity; more importantly, it may also become water-saturated so that it exsolves a separate fluid phase. The increasing fluid pressure might drive the melt into regions of lower pressure. Sisson and Bacon (1999) recognize four situations in which gas-driven filter pressing might drive melt down a pressure gradient:

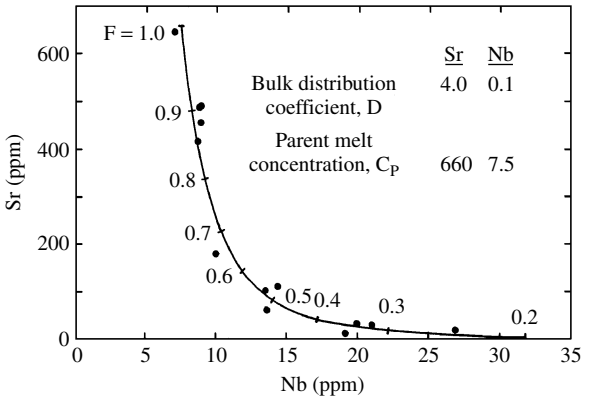


**12.5** Trace element variation diagram for a fractionating magma system. Variation is for compatible Sr and incompatible Nb in pumice inclusions (filled circles) in a compositionally zoned rhyolite-dacite ignimbrite. The pumices are geologic samples of the zoned preeruption magma chamber (similar to that in Figure 10.38), which experienced fractional crystallization of two feldspars, quartz, biotite, and Fe-Ti oxides (present as phenocrysts in the ignimbrite) having the indicated bulk distribution coefficients. The curved line was constructed from equation 12.1, which was used to calculate the value of $C_m$ for Sr and Nb as a function of $F$ using the indicated bulk distribution coefficients and parent melt concentrations. Adjustment of these two model parameters and proportions of fractionating crystals allowed the curve to be fitted to the analytical data. It must be remembered that, no matter how good the fit, the model parameters constitute only a *possible* set of conditions in the actual magma system. That is, the agreement between the data and the model does not prove these parameters actually existed. (From Best et al., 1995.)

a. Migration of residual melt in crystallizing lava flows and shallow crustal intrusions.
b. Expulsion of melt from partly crystallized or melted rock inclusions into the host magma.
c. Expulsion of residual melt from mostly crystallized magma into nearby cracks, perhaps created by hydraulic fracturing (Section 8.2.1). Thin dikes of evolved leucocratic aplite in more mafic host granitoids (Figures 7.48 and 9.3) are a likely example. Merely opening the fracture creates a pressure gradient that might suck residual melt out of the host magma, but exsolved fluid in the melt would enhance the gradient and melt separation.
d. A crystallizing mafic underplate beneath or near the base of a crustal magma chamber contributes evolved melt that can mix with the chamber magma (Figures 8.24 and 8.25).

4. **Convective melt fractionation:** Residual melts may have sufficient buoyancy to move out of the enclosing crystalline network. This mechanism became well established in the 1980s, partly as a result of model laboratory experiments using tanks of salt solutions (e.g., McBirney et al., 1985) and partly as a result of evidence for it found in rocks. Rather than gravitational compaction of a cumulate mat on the floor of a magma chamber, causing the interstitial residual melt to be pressed out, gravity may cause the melt to rise buoyantly out of the network of crystals because of its lower density. Bubbles of exsolved fluid would make them more buoyant. Ascending diapiric "fingers" of less dense residual melt, entraining some crystals, developed in Hawaiian lava lakes (Helz et al., 1989; see also Figure 8.23). Convective melt fractionation during sidewall crystallization in bottle-shaped intrusions is a well-accepted differentiation process in intermediate-composition magma chambers (Section 8.6.2; Figures 8.22 and 10.38).

### 12.2.2 Physical Separation of Immiscible Melts

Immiscible silicate melts were discovered in the early 1900s in the system MgO-$SiO_2$ (Figure 5.8). Further experiments as well as petrographic observations by the late 1900s had demonstrated the existence of immiscible silicate melts in other magmatic systems.

Many fresh, unoxidized tholeiitic basalts and some alkaline ones having high concentrations of FeO, $P_2O_5$, and $TiO_2$ and low MgO, CaO, and $Al_2O_3$ contain two compositionally distinct glasses lying interstitially between higher-T crystals. The two glasses, identifiable in thin section by contrasts in color and refractive index (Figure 12.6), are interpreted to have formed as two immiscible residual silicate melts (Philpotts, 1982). In slowly cooled intrusions, these two melts and any en-

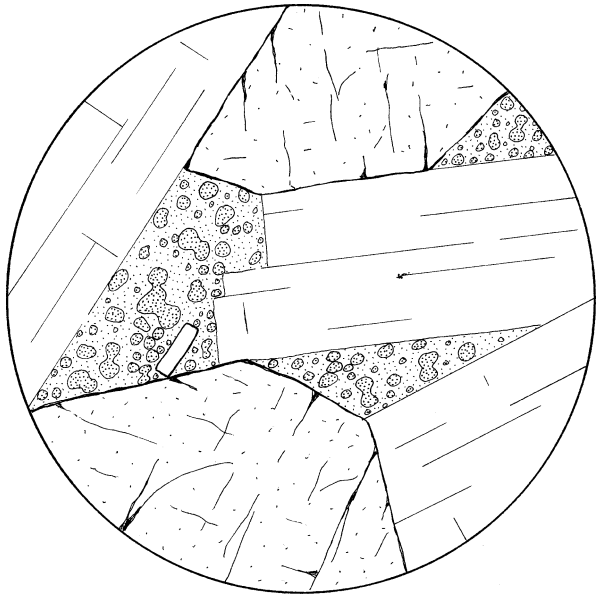

**12.6** Immiscible silicate melts in basalt. Interstitial spaces between larger plagioclases and pyroxenes are of a **mesostasis** that was two immiscible melts but now consists of clear silicic glass hosting small globules of Fe-rich glass (darker stippling). Globule diameters are on the order of a few micrometers.

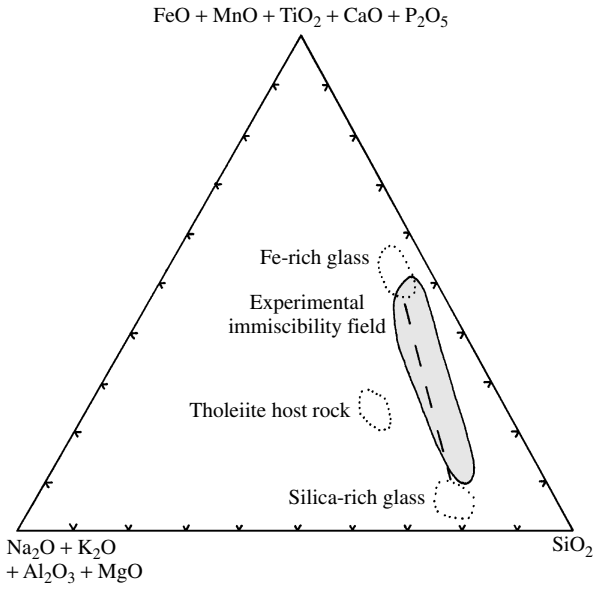


**12.7** Compositions of immiscible melts in tholeiite basalt. Dotted lines enclose analyzed immiscible melts (now glasses, connected by dashed tie line) and host rock compositions. Shaded area is field of immiscible melts in model system $KAlSi_2O_6$-$Fe_2SiO_4$-$SiO_2$. (Redrawn from Philpotts, 1982.)

trained crystals might segregate, as a result of density contrasts, into substantial volumes of magma. Crystallization could yield, on the one hand, an Fe-rich rock composed essentially of Fe-Ti oxides, apatite, and Fe-rich pyroxene and, on the other hand, a granitic rock (Table 12.3 and Figure 12.7). Extremely rare nelsonite, a rock made mostly of Fe-Ti oxides and apatite, may also represent a segregated immiscible melt.

Field, fabric, and compositional relations indicate some alkaline magmas in laccoliths in eastern Montana unmixed into conjugate syenite and shonkinite (mafic syenite) (Table 12.3). Each rock consists of clinopyroxene, olivine, biotite, and alkali feldspar of similar chemical composition, but in different modal proportions, as would be expected if the two rocks formed from immiscible melts and suspended crystals that were all in equilibrium. The syenite occurs as blobs within shonkinite, reflecting their original two-liquid status. These two-liquid shapes together with trace element partitioning in the syenite and shonkinite rule out crystal-melt fractionation as a mechanism to create the two rock compositions.

Petrographic and experimental investigations have unequivocally established the immiscibility of sulfide and silicate melts. Concentrations of only a few hundred parts per million of S are sufficient to saturate basaltic melts. Greater concentrations result in separation of a sulfide melt that is chiefly Fe and S with minor Cu, Ni, and O that can ultimately crystallize to pyrrhotite, chalcopyrite, and magnetite. Although trace amounts of Ni are strongly partitioned into crystallizing olivine in basaltic melts, the uptake into an immiscible sulfide liquid is 10 times greater; for Cu it is 100 to 1000 times greater. Pb and Zn apparently tend to remain in the silicate melt. Sulfide-silicate melt immiscibility has significant implications for the genesis of some magmatic and hydrothermal ore deposits.

**Table 12.3** Chemical Compositions of Paired Glasses and Rocks Formed by Separation of Immiscible Melts

| | 1 | 2 | | 3 | 4 |
|---|---|---|---|---|---|
| $SiO_2$ | 41.5 | 73.3 | | 45.88 | 50.84 |
| $TiO_2$ | 5.8 | 0.8 | | 1.53 | 1.12 |
| $Al_2O_3$ | 3.7 | 12.1 | | 11.32 | 16.45 |
| $Fe_2O_3$ | — | — | | 6.60 | 4.40 |
| FeO | 31.0t | 3.2t | | 7.56 | 5.04 |
| MnO | 0.5 | 0.0 | | 0.15 | 0.12 |
| MgO | 0.9 | 0.0 | | 6.50 | 3.78 |
| CaO | 9.4 | 1.8 | | 11.42 | 7.28 |
| $Na_2O$ | 0.8 | 3.1 | | 2.06 | 2.97 |
| $K_2O$ | 0.7 | 3.3 | | 5.12 | 7.18 |
| $P_2O_5$ | 3.5 | 0.07 | | 1.84 | 1.07 |
| Total | 97.8 | 97.67 | | 99.98 | 100.25 |
| *Q* | 13.7 | 37.8 | Cs | 2.75 | 3.18 |
| *Or* | 4.1 | 20.0 | Rb | 762 | 125 |
| *Ab* | 6.8 | 26.9 | Ba | 36,000 | 50,534 |
| *An* | 4.5 | 8.7 | Th | 14.24 | 14.27 |
| *Di* | 17.2 | 0.0 | U | 3 | 2.81 |
| *Hy* | 21.8 | 2.5 | La | 824 | 600 |
| *Il* | 11.0 | 1.5 | Ce | 128.1 | 116.4 |
| *Ap* | 8.1 | 0.2 | Sr | 1591.7 | 1627.5 |
| *Mt* | 11.5 | 1.2 | Sm | 10.0 | 7.4 |
| *C* | | 0.3 | Hf | 2.91 | 2.75 |
| | | | Eu | 2.00 | 1.68 |
| | | | Dy | 35.7 | 30.8 |
| | | | Lu | 0.32 | 0.25 |
| | | | Co | 26.25 | 13.74 |
| | | | Cr | 210.3 | 195.5 |
| | | | Ni | 622 | 39 |
| | | | Sc | 21.4 | 8.8 |
| | | | V | 1500.5 | 1437 |

1 and 2, Average oxide and normative composition of glasses in mesostases in tholeiitic basalts. (Oxide data from Philpotts, 1982.)
3 and 4, Oxide and trace element compositions of shonkinite (3) and "blob" syenite (4), Montana. Data from Kendrick and Edmond (1981).

Carbonatite. In several locales around the world, small volumes of carbonatite occur with silica-undersaturated alkaline rocks. **Carbonatite** contains >50% carbonate minerals, usually calcite. Since 1960 the nephelinitic Oldoinyo Lengai volcano in Tanzania has erupted alkali carbonate lavas and pyroclastics. Earlier arguments whether carbonatite is truly a magmatic rock were laid to rest by this eruption and discovery of other carbonatite volcanic rocks. Table 12.4 reveals the extreme composition of carbonatites; in alkali carbon-

**Table 12.4** Chemical Composition of Carbonatite Segregations in Nephelinitic Ash Particles, the Two Representing Immiscible Melts, Oldoinyo Lengai, Tanzania

| | CARBONATITE | NEPHELINITE |
|---|---|---|
| $SiO_2$ | 3.17 | 43.97 |
| $TiO_2$ | 0.10 | 2.34 |
| $Al_2O_3$ | 1.05 | 7.96 |
| FeOt | 1.33 | 11.03 |
| MnO | 0.33 | 0.37 |
| MgO | 0.3 | 4.68 |
| CaO | 15.52 | 17.77 |
| $Na_2O$ | 30.05 | 4.91 |
| $K_2O$ | 5.35 | 1.57 |
| $P_2O_5$ | 1.28 | 0.32 |

Data from Dawson et al. (1994).

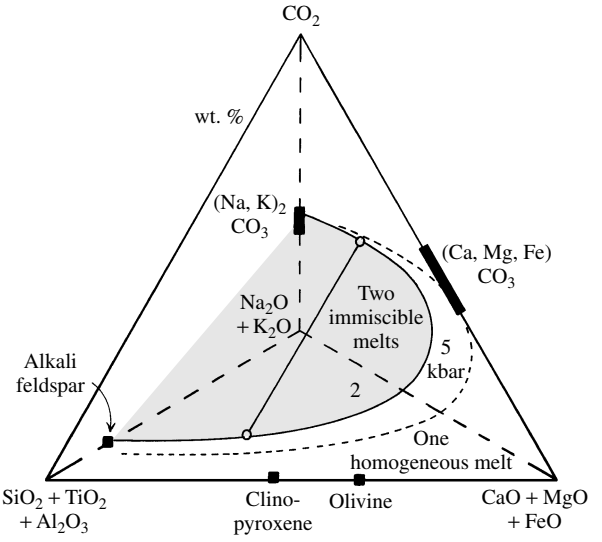


**12.8** Immiscible melts in a carbonated silicate system. The shaded area represents the polythermal stability field of two immiscible melts below the arcuate 2-kbar solvus. Compositions of coexisting carbonate and silicate segregations in Oldoinyo Lengai volcanic ash from Table 12.4 shown by open circles connected by tie line. Segregation of these two immiscible melts from an initially homogeneous melt above (to the right of) the solvus may have occurred with decreasing $T$ and $P <$ 2 kbar. Solvus at 5 kbar is dashed line. Solid squares and rectangles represent compositions of minerals that might be stable in carbonated silicate systems. See also Lee and Wyllie (1997). (Redrawn from Kjarsgaard and Hamilton in Bell, 1989.)

atite, there is <3.2 wt.% $SiO_2 + Al_2O_3$ but major concentrations of SrO, BaO, $SO_3$, Cl, F, and, of course, $CO_2$. Carbonatites host no fewer than about 275 documented minerals in addition to carbonate minerals; other common minerals include apatite (repository of most REEs), magnetite, fluorite, pyrochlore (an Nb oxide that contains substituting Ta, Ti, Zr, Th, U, Pb, Ce, Ca, Sr, Ba), and alkaline amphibole. Most carbonatites are intimately associated with phonolite and more commonly with olivine-poor nephelinite.

Nd and Sr isotope ratios (Bell, 1989) unequivocally demonstrate that the ultimate source of carbonatite magmas is the mantle, probably long-lived, metasomatically enriched subcontinental lithosphere. Tangible samples of such a source are represented by rare garnet-phlogopite-calcite lherzolite inclusions in carbonatite tuffs. Experiments confirm that carbonatite partial melts can exist under special mantle conditions (Figure 11.5).

In June 1993 Oldoinyo Lengai erupted carbonatite lava and ash that contained nephelinitic spheroids that themselves contained alkali carbonatite segregations (Table 12.4). These are obviously immiscible silicate-carbonatite melts that separated from a carbonated silicate magma at low $P$ (Figure 12.8).

### 12.2.3 Fluid-Melt Separation: Pegmatites

Experiments and observations of rocks indicate that aqueous and carbonatitic fluids in equilibrium with melts in magmatic systems contain significant concentrations of many chemical components, such as Si, Na, K, Fe, and many incompatible elements. Exsolution of fluid solutions from the coexisting melt is therefore a significant means of modifying its composition. In the terminal stages of the solidification of many intrusions of granitic magma the creation of bodies of pegmatite is believed to be critically dependent on separation of an aqueous fluid phase from the residual water-saturated granite melt; this is the Jahns and Burnham (1969) model of pegmatite formation (see also, for example, Thomas et al., 1988).

**Pegmatite** is an unusually coarse-grained magmatic rock. Although giant crystals measured in meters occur in some (Figure 7.11), grain size is usually highly variable, and fine-grained phaneritic felsic rock (aplite) is commonly an intimate part (Figure 12.9). Large vugs (open cavities) are common. Most pegmatites are syenitic and granitic; more mafic ones also occur but ultramafic pegmatites are rare. Pegmatite bodies are relatively small—ranging from 1 m or less to a few hundred meters—and most occur as pods or lenses around the margins of nearby larger, deep-seated plutons, commonly extending from the pluton itself into the adjacent country rocks. In the famous Black Hills district of South Dakota (e.g., Norton and Redden, 1990), an estimated 24,000 pegmatite bodies are found over an area of 700 $km^2$, whereas the roof of the underlying comagmatic peraluminous granite is exposed over 100 $km^2$. **Simple pegmatites** consist essentially of a minimum-$T$ granite composition (Figures 5.24–5.26) of

**12.9 Pegmatite,** San Diego mine, Mesa Grande district, San Diego County, California. Layered aplitic footwall underlies coarser pegmatitic upper part. Fringes of black tourmaline, especially evident at top of pegmatite, probably denote contemporaneous crystallization along footwall and hangingwall portions. Giant graphic microcline crystals radiate up from the footwall aplite, not down from the hangingwall as the Jahns-Burnhall model predicts. Scale card in center of photo is 9 cm long. (Photograph and caption courtesy of David London.)

albite, quartz, perthite, and possible minor muscovite, tourmaline, and Fe-Mn garnet. Rare (2% in the Black Hills) **zoned pegmatites** have an internal, layerlike zonation of fabric and mineralogical composition (Figures 12.9 and 12.10) that locally may be transected by late, metasomatic replacement bodies. A small proportion of these internally differentitated, zoned pegmatites, referred to as **complex pegmatites,** have relatively high concentrations of P, Cl, F, and B, as well as large-ion lithophile, rare earth, and other incompatible elements strongly partitioned into the residual melt during fractional crystallization of the parent granitic magma. For example, Li in the Black Hills granite averages about 30 ppm but in complex pegmatites can be as much as 7000 ppm, an enrichment factor of 233. These high concentrations stabilize minerals such as topaz (high concentrations of F), spodumene, lepidolite and amblygonite (Li), beryl (Be), columbite-tantalite and pyrochlore (Nb, Ta, Ce, Y), cassiterite (Sn), pollucite (Cs), monazite (Ce, La), zircon (Zr), and uraninite (U). Obviously, these complex pegmatites can be economically very valuable, but simple ones are also exploited for sheet muscovite (electrical and thermal insulators, such as in bread toasters) and large volumes of quartz and feldspar used in the glass and ceramic industries.

In the classic Jahns-Burnham pegmatite model, zoned pegmatites develop by inward solidification and differentiation of a lens-shaped body of water-saturated granite melt that produces the contrasting and commonly asymmetric mineralogical and textural zones. The outer margin, locally modally layered, is much like the host granite or syenite but abruptly coarser in grain size, by as much as several orders of magnitude. Inward from the margin are graphic intergrowths of feldspar and quartz (Figure 7.20) and comb layers of crystals (Figure 7.47) that are commonly branching, inward-flaring, plumose, and locally of giant size and oriented perpendicular to pegmatite walls. Large internal portions are wholly quartz or feldspar or giant crystals of exotic minerals (Figure 7.11). Crystallization can continue to $T$ as low as 300°C.

Many aspects of pegmatite development, particularly the large crystal size and other aspects of the internal fabric as just described, are controversial. Kinetic factors may be critically significant (London, 1992; Morgan and London, 1999).

## ❋12.3 OPEN-SYSTEM DIFFERENTIATION: HYBRID MAGMAS

### 12.3.1 Magma Mixing

If two or more dissimilar parent magmas blend together, a hybrid daughter magma compositionally intermediate between them is produced. Magmas can be derived from different sources, such as basaltic magma from the upper mantle and silicic magma from the deep continental crust, or they may have had a common parent magma but followed different evolutionary tracks, such as the contrasting magmas in a compositionally zoned chamber (Figure 10.38). Other scenarios are possible. Initially, dissimilar magmas are physically **mingled.** If solidification occurs soon afterward, the composite rock has layers, lenses, pillow-shaped blobs, or more irregularly shaped bodies in a dissimilar matrix (Figures 7.42, 8.25, 12.11). Rocks formed by mingling of magmas retaining their contrasting identity are evident on scales ranging from a thin section to large outcrops. After mingling, magmas may become **mixed** on an atomic scale by diffusion, if sufficient time and thermal energy are available, forming an essentially homogeneous melt. Homogenization and equilibration of crystals from the two batches of magma take a longer time. Hybridizing magmas can be as different as basalt and rhyolite or differ by as little as a few weight percentages in major elements.

Long after its first proposal by R. Bunsen in 1851, magma mixing became the subject of contentious debate in the 1920s and 1930s. C. N. Fenner advocated that the mixing of rhyolite and basalt magmas could produce the spectrum of compositions found in many magmatic rock suites, whereas N. L. Bowen persuasively advocated crystallization-differentiation (crystal-melt fractionation) as the dominant process of magmatic diversification. Writers of standard petrology textbooks of that time either made no mention whatsoever of mixing (Daly, 1968) or wrote only one brief sen-

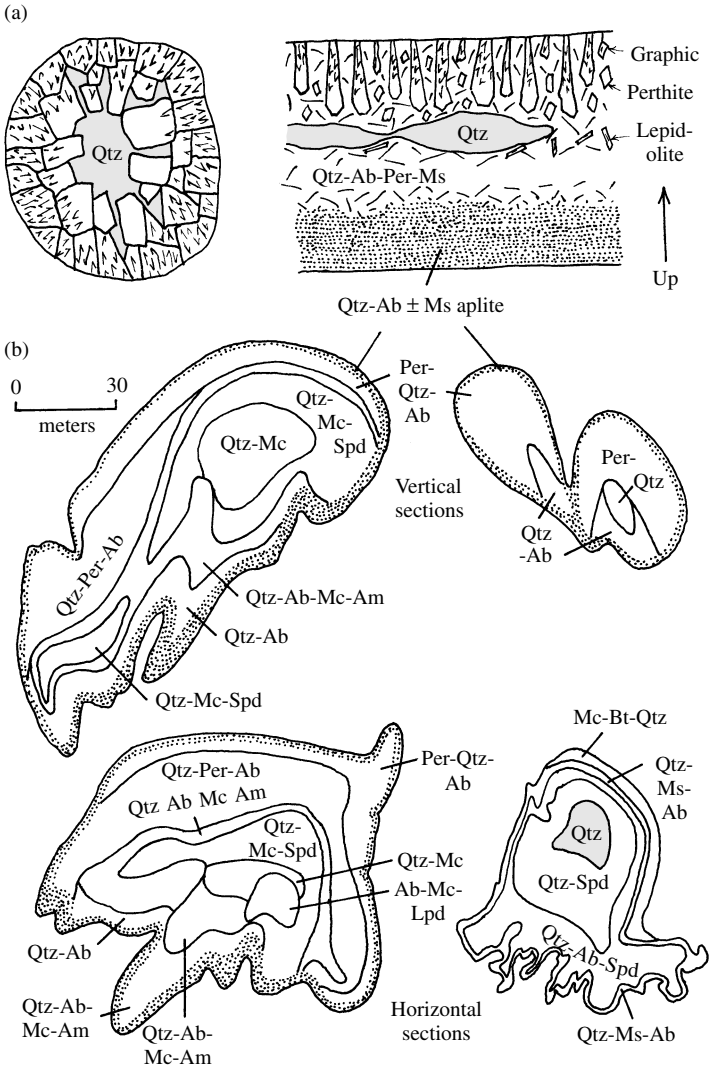


**12.10** Schematic sections through zoned **pegmatite** bodies. (a) Body on left is several centimeters in diameter; on right is 1 to 2 m thick. Massive quartz is shaded; largest crystals are of quartz-perthite graphic intergrowth near pegmatite margin grading inward to perthite alone. (Redrawn from Jahns and Burnham, 1969.) (b) On the left are two sections of same body. Ab, albite; Am, amblygonite; Bt, biotite; Lpd, lepidolite; Mc, microcline; Ms, muscovite; Per, perthite; Qtz, quartz; Spd, spodumene. (Redrawn from Norton and Redden, 1990.)

tence (Grout, 1932): "Some mixing of magmas . . . may develop . . . but the process is probably rare." Since the late 1970s, however, petrologists have recognized widespread evidence for magma mixing so that it has now gained prominence as a significant differentiation process.

Compositionally dissimilar magmas are usually also dissimilar in *T* and physical properties, particularly apparent viscosity. Such contrasts are involved in many mechanisms of hybridization within intrusions and conduits feeding volcanic eruptions and even in flowing lava. The following are a few possibilities for mingling and possibly mixing:

1. During evacuation and flow through narrow conduits (e.g., Snyder et al., 1997): Erupted magmas form mingled lavas and pyroclasts.
2. Convective overturn and stirring in a magma chamber when underlying, initially denser mafic magma cools and exsolves volatile fluids, making it less dense than the overlying silicic magma: The underlying vesiculating magma develops m-scale Rayleigh-Taylor instabilities (compare Figure 9.15), causing detachment of buoyant blobs (Figure 8.24), some of which may become mingled mafic inclusions within the felsic host if solidification is rapid; longer residence in hot magma allows mixing.
3. Plumelike rising of hot, replenishing magma into an evolving chamber: This likely happens in basaltic oceanic-ridge systems as episodically replenishing primitive magma mingles and mixes with cooler magma that has evolved somewhat by crystal fractionation (Figure 12.12).


**12.11 Mingled** rhyolite and basalt lava, Gardiner River, Yellowstone National Park, Wyoming. In thin section, euhedral plagioclase and pyroxene phenocrysts from the basalt lava (darker colors) coexist with corroded quartz and sanidine phenocrysts from the rhyolite lava. (U.S. Geological Survey photograph courtesy of R. E. Wilcox and Louise Hendricks.)

Multiple lines of independent evidence can strengthen the mixing interpretation but are never sufficient to prove this process occurred. Disequilibrium textures in a rock that appears to be homogeneous but was produced by mixing of felsic and mafic magmas include the following:

1. Complex resorption and overgrowths in phenocrysts in quickly cooled volcanic systems, such as spongy zones within plagioclase (Figure 7.19) and rapakivi overgrowth of plagioclase on alkali feldspar (Figure 7.18): Normal fractional crystallization of ternary feldspars during cooling would not create rapakivi texture. However, these overgrowth textures can possibly be produced by changes in $P$ or water fugacity in the magma system.
2. Anhedral, partially dissolved quartz rimmed by an aggregate of clinopyroxenes (Figure 6.20): The unstable quartz grains can be derived from felsic magma mingled with more mafic magma or from quartz-bearing rock assimilated (discussed later) into the mafic magma in which clinopyroxene is a stable phase.

Compositional evidence for magma mixing in the history of a rock or rock suite includes the following:

1. Disequilibrium phases, such as coexisting quartz and Mg-olivine or calcic and sodic plagioclase.
2. Phenocryst-hosted glass (melt) inclusions that are compositionally unlike surrounding matrix glass.
3. Distinctive patterns on variation diagrams: Simple magma mixing produces straight-line trends on element-element variation diagrams (Figure 12.3 and Special Interest Box 12.1). However, because of limited thermal energy in most magma systems, only limited mixing occurs. Consequently, compositions of the rocks produced by mixing are generally only displaced slightly away from the parent magma composition toward the mixing magma composition.

If mixing proceeds to a homogeneous hybrid magma, its composition, $C_b$, can be expressed by a simple **mass balance equation** of the compositions of the

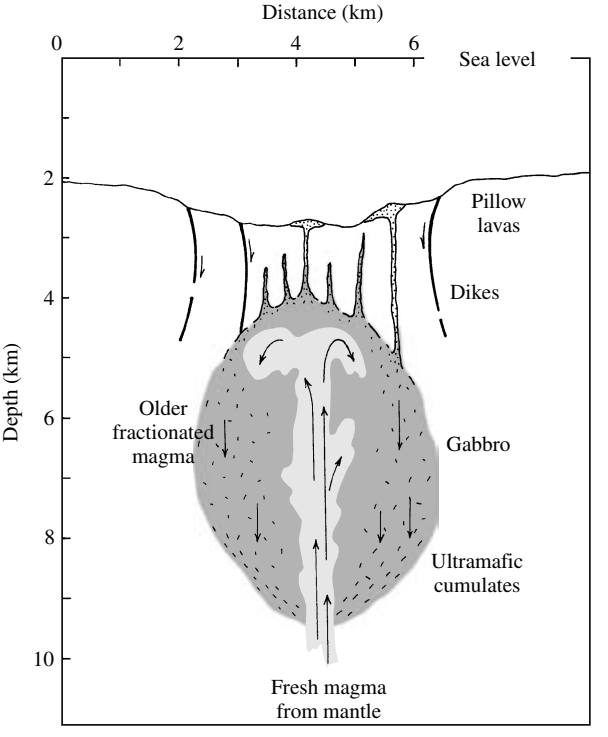


**12.12** Schematic cross section through an episodically replenished oceanic rift magma chamber. Replenishing primitive magma from the mantle rises buoyantly into the chamber and mixes with cooler, denser, Fe-rich fractionated magma. Gabbro made of olivine, pyroxenes, and plagioclase crystallizes on the chamber walls; olivines and pyroxenes form ultramafic cumulates on the chamber floor. Evolving basaltic magmas are episodically injected through fissures in the overlying extending roof, forming feeder dikes for submarine extrusions, mostly pillow lavas. (Redrawn from Bryan and Moore, 1977.)

two end-member parent magmas, $C_x$ and $C_y$; the mixing proportion, $F_x$, represents the weight fraction of one of the magmas

$$12.2 \quad C_b = C_x F_x + C_y(1 - F_x)$$

Magma mixing, depending on how disparate the magmas are, may be accompanied by crystallization of new phases stabilized by the compositional and thermal properties of the hybrid system.

### 12.3.2 Assimilation

After leaving its source, a batch of ascending buoyant primary magma can encounter wall rock of different composition, especially basaltic magmas from mantle sources rising into sialic rocks of the continental crust and any silicate magma encountering Ca-rich limestone or Al-rich shale or their metamorphic equivalents. Magmas interact with their surroundings in an attempt to attain chemical and thermal equilibrium, especially where they slow or even stop in subterranean storage chambers. Hot country rocks are by no means inert to hotter, contrasting magma.

Incorporation of solid rock into a magma of different composition is the process of **assimilation;** it produces a **contaminated magma,** which is also hybrid, like mixed magmas. The contaminant can be country rock around the magma chamber or xenoliths within the magma. Assimilation may initially involve simple physical dispersal of xenoliths and xenocrysts into the magma, such as Precambrian zircons in Miocene rhyolite. Depending on magma and foreign material compositions and temperatures and available time, the foreign material chemically equilibrates with the melt to varying degrees. Minerals may selectively dissolve into the melt and contaminant ions incorporate into it by time- and $T$-dependent diffusion. Commonly, assimilation involves mixing with melts created by melting of the contaminant rock.

The thermal and chemical principles of assimilation were enunciated by Bowen (1928) many decades ago. Assimilation requires thermal energy, the source of which can only be the magma itself. Heat from the magma has two sources:

1. That released during cooling to lower $T$
2. The latent heat of crystallization

As few magmas appear to be superheated above their liquidus $T$, the available heat for assimilation is derived by concurrent crystallization and cooling of the magma below its liquidus. Section 11.1.1 indicated that the mass of lower continental crustal rock melted by a mass of intruded hotter basaltic magma is of the same order of magnitude, more of this magma would be required in the cooler shallower crust. Obviously, hotter, more mafic magmas have greater assimilative potential. But transfer of heat from a magma body into adjacent cooler rock leads to solidification at its contact, building an armor of solid magmatic rock that inhibits further assimilation. Pieces of stoped country rock (Section 9.4.3) within a body of magma afford a significantly greater surface area over which heat can be transferred and assimilative processes operate than the country rock. Volatile fluids liberated from heated country rock may contaminate volatile-poor magma with Si, K, Na, and other elements, as the fluid solution is absorbed into it.

The fate of assimilated crystals depends on their composition and that of the parent melt. Provided sufficient heat is available, a crystalline phase dissolves if the silicate melt is not already saturated with respect to that phase. Thus, quartz xenocrysts can dissolve on a time scale of days in basaltic melts in which the activity of silica is $<1$ (the usual case); melts so contaminated are enriched in silica. Alkali feldspar, biotite, and hornblende in granite assimilated by basalt follow a similar fate, but the details differ. Assimilation of granite in basalt magma promotes crystallization of some of the phases it would have normally precipitated and along similar lines of liquid descent; however, felsic derivatives are more abundant. Crystals react with a melt if they would have precipitated from the magma at higher $T$. Thus, physically ingested crystals of Mg-rich olivine into Makaopuhi basalt magma at $T = 1075°C$ and 1 atm (Plate III), where olivine is no longer stable, would induce precipitation of additional stable pyroxene by a reaction relation with the melt. Xenocrysts of clinopyroxene—perhaps derived from incorporated basalt xenoliths—in a granodiorite melt precipitating stable hornblende but not pyroxene would be expected to react with the melt, forming, by ionic diffusion, a reaction rim of hornblende surrounding and possibly eventually replacing the unstable clinopyroxene. Assimilation of quartz xenocrysts, perhaps from ingested blocks of sandstone, into a quartz-saturated granitic melt simply adds more modal quartz to the final granite. Assimilation of Al-rich minerals into basalt magma stabilizes calcic plagioclase at the expense of calcic clinopyroxene, so that leucocratic orthopyroxene gabbro (norite) magmas might form.

Evidence for magma contamination in the history of a rock is generally only permissive. The presence of xenocrysts (e.g., quartz in basalt, Figure 6.20) and xenoliths in a magmatic rock may suggest they are contaminants, but xenocrysts can also originate by mixing of dissimilar magmas, and foreign material can be incorporated late into the magma with minimal contamination of the melt. Strained xenocrysts that show undulatory optical extinction under cross-polarized light in thin section or other solid-state strain effects are especially useful in distinguishing assimilated solid material from phenocrysts in mixed magmas.

Sr and O isotopic signatures (as well as Nd and Pb) can also provide permissive evidence for assimilation of continental felsic crust into primitive mantle-derived basaltic magmas. Precambrian felsic rocks have relatively low Sr but high Rb; over time, $^{87}Rb$ decays and elevates the $^{87}Sr/^{86}Sr$ ratio (Section 2.6.2) to well above that of primitive mantle-derived partial melts, which are typically about 0.703–0.704 (Figures 2.26 and 2.27). If mantle-derived magmas assimilate old continental crust, their ratio is elevated. $^{18}O$ in mantle source rocks and their basaltic partial melts is ~6‰, in contrast to sedimentary rocks, in which $\delta^{18}O$ = 10−32‰ (Figure 2.24; Section 2.6.1). Consequently, mantle-derived magmas that assimilate sedimentary rocks are enriched in $^{18}O$. Mantle-derived magmas that assimilate old felsic rocks *and* sedimentary rocks (or their metamorphic equivalents) are enriched in both $^{87}Sr$ and $^{18}O$ (Figure 12.13).

## ✲12.4 DIFFERENTIATION IN BASALTIC INTRUSIONS

Because of their relatively low viscosity and slow cooling, intrusions of basaltic magma potentially provide an opportunity to evaluate the role of crystal-melt fractionation in magmatic differentiation. In this section, three types of intrusions are examined to determine the extent to which fractionation does occur and the nature of the evolved fractionated magmas and whether intrusions behave as closed systems or other differentiation processes are also involved. If they can be accurately interpreted, these intrusions provide tests of petrologists' theoretical models and small-scale, time-restricted laboratory experiments on crystal-melt systems. Knowledge gained from mafic intrusions constrains models purporting to account for compositional variations in extruded lavas that erupted sequentially from a particular volcanic center and possibly derived from underlying differentiating storage chambers.

### 12.4.1 Palisades Sill

Differentiation in smaller subhorizontal sheets is considered first, using the Palisades sill as an example. The diabase-granophyre association in such sheets was the basis for the emphasis by Bowen (1928) that closed-system crystal-melt fractionation is the most important process of magmatic differentiation.

The Palisades diabase sill is a subhorizontal sheet intrusion exposed for at least 80 km along the Hudson River opposite New York City. It is one of ennumerable early Jurassic basaltic dikes and sills intruded along the east coast of North America during the breakup of the American and African continental plates (Figure 9.7b; see also Olsen, 1999). Whether or not it is everywhere a concordant sheet does not detract from the fact that it, like many others, displays more or less regular variations in bulk chemical, modal, and mineral composition and fabric throughout a vertical extent of hundreds of meters (Figure 12.14). Inward solidification of the sill progressed to a "sandwich horizon" near the top of the sill where the most evolved residual magma crystallized to patches of granophyric pegmatite. In this felsic differentiate, grain size is uneven, ranging

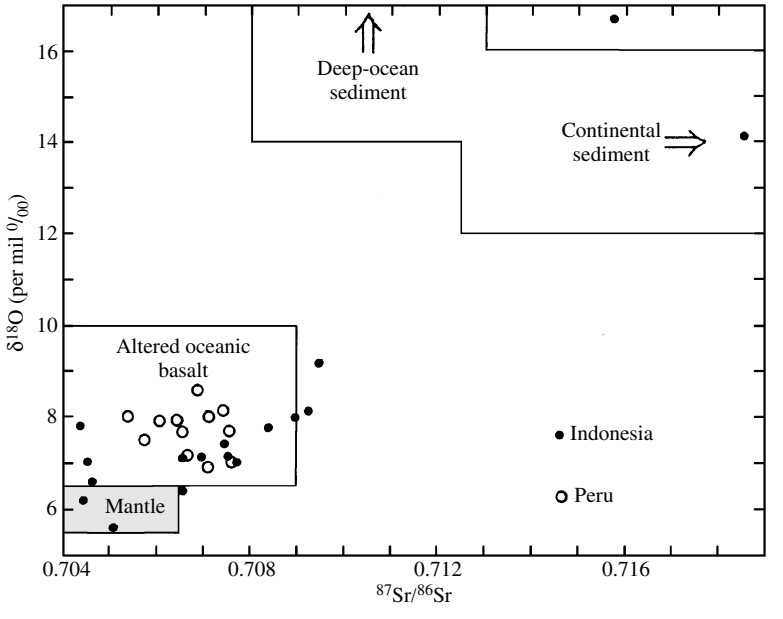


**12.13** Oxygen and Sr isotopic composition of andesites from the Banda arc, Indonesia, and the Andean arc, southern Peru. Note two Indonesia samples in upper right. Range of composition of potential sources shown. (Redrawn from Magaritz et al., 1978.)

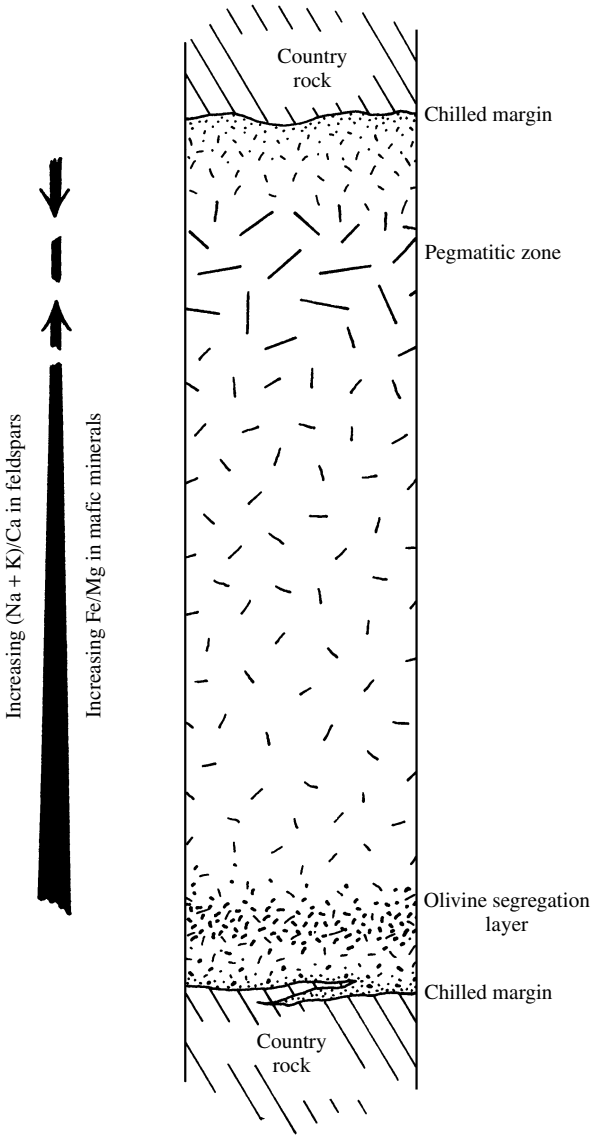


**12.14** Schematic cross section through an idealized diabase-granophyre sill. Lengthening dash lines indicate increasing grain size into pegmatitic granophyre zone.

from the micrographic quartz-alkali feldspar intergrowth typical of granophyre (Figure 7.21) to bladelike Fe-rich clinopyroxenes several centimeters long. An olivine-rich layer (10–25% of rock) having abundant pyroxene is located 10–25 m above the floor of the sill.

The Palisades sill was interpreted for decades to be a simple product of closed-system differentiation driven by gravity settling of denser olivines and pyroxenes to the intrusion floor. However, several investigations in the late twentieth century (see, for example, Gorring and Naslund, 1995) showed that this hypothesis is flawed. Studies of this and other similar differentiated sills indicate episodic recharge of fresh magma into the crystallizing fractionating bodies: That is, they were open magma systems.

The simple gravity settling hypothesis for the Palisades, wherein precipitating olivine crystals "rain down" through the crystallizing magma to form the olivine-rich layer, is rejected for several reasons:

1. The olivine-rich layer pinches and swells along the exposed extent of the sill and is locally absent.
2. The proportion of olivine increases abruptly into the layer from essentially zero above it, implying an unlikely very efficient gravitational settling "sweep" from above.
3. Olivines in the layer are far more Fe-rich ($Fo_{55–70}$) than expected from the olivine composition ($Fo_{80}$) in the finer grained, chilled margin, presumed to represent the quenched parent magma. Moreover, olivines in this chilled margin are embayed and were presumably unstable when the magma solidified.
4. Local internal "chilled" contacts within the sill and significant reversals or discontinuities in elemental trends in vertical sections (Figure 12.15) suggest multiple injection of additional magma into the fractionating magma system. One of these fresh draughts of magma is hypothesized to have carried a large proportion of suspended olivine that, during emplacement into the flat sheet, was smeared out as the olivine-rich basal layer.

The composite intrusion hypothesis seems intuitively probable because during the calculated several-hundred-year solidification time of the sill (Section 8.4.1) new ascending batches of magma feeding the overlying flood lavas may have intersected the horizontally widespread sill.

Despite the apparent magma replenishment and mixing, the Palisades magma has an overall vertical elemental variation that is readily explained by fractionation of plagioclase and clinopyroxene, the major minerals present throughout the sill. But the exact physical mechanism of the fractionation is uncertain. Because of possible restrictions imposed by the plastic yield strength of the melt (Section 8.2.2), gravitational settling of independent crystals of plagioclase and clinopyroxene through the magma may have been limited. But if this restriction was valid, how does one explain the highly asymmetric position of the late felsic differentiates near the top of the sill (Figure 12.14)? This seems to imply that gravity acted in some way. Perhaps large clumps of gravitationally unstable crystals growing near the roof fell to the floor of the crystallizing sill, augmenting the mat of crystals growing there. Buoyant residual melt could have escaped from the interstices of the mat of plagioclase and pyroxene grains, as a result of compaction under its own weight (filter pressing), or convective melt fractionation, or both. Displaced residual melt apparently accumulated near the roof of the sill, beneath downward crystallized magma, in the sandwich horizon, there forming the most-evolved Fe-rich granophyre.

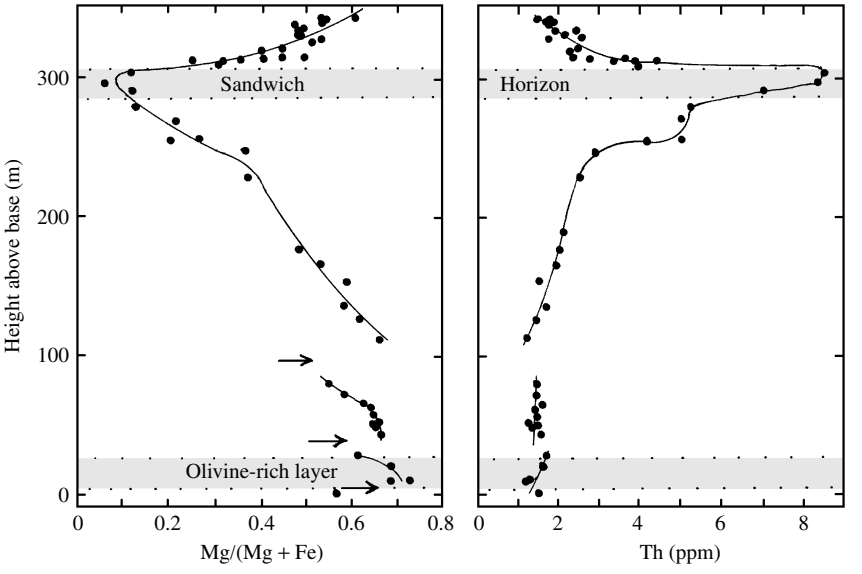


**12.15** Chemical variation in rocks of the Palisades sill, New Jersey. Discontinuities in Mg/(Mg + Fe) ratio at arrows is consistent with influx of new, less differentiated magma into the sill. (Data from Shirley 1987.)

### 12.4.2 Layered Intrusions

**Layered mafic intrusions** have attracted the attention of petrologists for many decades (Cawthorn, 1996). Most of the large intrusions are of Precambrian age (Table 12.5), and the largest of these is the colossal Bushveld complex in South Africa which crops out over an area of about 65,000 $km^2$; the estimated 0.5-million $km^3$ of basalt magma that formed this 2-Ga intrusion was no doubt related to the head of a decompressing mantle plume. The volume of smaller intrusions, such as the early Tertiary Skaergaard intrusion in southeast Greenland (170 $km^3$), is comparable to that of some floods of plateau-forming basalt lava (Section 10.2.2).

Layering and Cumulus Fabric. Layering in these intrusions (Figures 7.43–7.45) is as pervasive and distinctive as stratification in sedimentary sequences. Single layers range from millimeters to hundreds of meters in thickness and from meters to tens, and even hundreds, of kilometers in lateral extent. In the Bushveld complex, the Merensky Reef—a pyroxenitic layer 1 to 5 m thick that is the chief global resource of platinum—extends along strike for nearly 150 km in the eastern part of the complex and 190 km along strike in the western part,

**Table 12.5.** Large Layered Intrusions

| Name, Location | Age (Ma) | Remarks |
|---|---|---|
| Skaergaard, Greenland | 55.7 | 55 $km^2$; >3.5 km thick (see Figure 13.23) |
| Rum, Scotland | 61–58 | 115 $km^2$; >2 km thick (see Figure 13.23) |
| Duluth, Minnesota | 1100 | More than a dozen layered intrusions exposed over 5000 $km^2$ |
| Muskox, Northwest Territories, Canada | 1270 | Canoe-shaped, 11 × 150 km (Figure 12.17); associated with the Mackenzie dike swarm (Figure 9.7a) |
| Sudbury, Ontario | 1850 | 1100 $km^2$ |
| Bushveld, South Africa | 2050 | Largest on Earth: 65,000 $km^2$ and 7–9 km thick; exceptional lateral continuity of individual layers |
| Jimberlana, Western Australia | 2370 | End-to-end canoe-shaped complexes averaging 1.5 km wide and 180 km long underlain by connecting dike |
| Great Dyke, Zimbabwe | 2460 | Four end-to-end canoe-shaped layered complexes 4–11 km wide and 550 km long underlain by a connecting feeder dike |
| Stillwater, Montana | 2700 | 8 × 55 km and ~7 km thick; only basal ultramafic cumulates and overlying gabbroic and anorthositic rocks preserved |
| Windimurra, Western Australia | 2800 | 35 × 85 km in area and 5–13 km thick; only slight differentiation |

Data from Hatton and von Gruenewaldt (1990) and Cawthorn (1996).

about 300 km distant. Layering is most conspicuously defined by variations in relative proportions of minerals, defining modal layering. Gradational variations within a single layer, from top to bottom, may be obvious, forming graded modal layers. Some layers are graded in grain size. Rhythmic layering, defined as a sequence of recurring similar layers, is common.

Another aspect of the fabric of layered intrusions parallels that of clastic sedimentary deposits. In sandstones, a textural distinction between accumulated sand grains and secondary cement surrounding them is generally obvious. In cumulate rocks of layered intrusions, a similar distinction may be obvious between collected early formed **cumulus grains** and **intercumulus** mineral matter that formed later around them. This magmatic "cement" filling space between cumulus grains was precipitated from the intercumulus melt initially entrapped during accumulation of cumulus grains or from a later, modified melt percolating through the cumulate pile (Figure 12.16). On the floors of magmatic intrusions, cementation and overgrowth compete with compaction in "densifying" the cumulus aggregate, eliminating the intercumulus melt (Hunter, 1996). For a recent discussion of the validity of the cumulate paradigm see Morse (1998).

Cumulates on floors of layered intrusions do not necessarily reflect gravitational settling, as once widely believed. For example, the Archean Stillwater complex of Montana has layers of cumulus chromite grains (about 0.25-mm diameter, density 4.4 g/cm$^3$) near the base that grade upward into larger, less dense cumulus olivine grains (0.7–3.0 mm, 3.3 g/cm$^3$). As settling velocity, according to Stokes's law (Section 8.3.3), is proportional to the square of the particle size but only to the first power of the density contrast with the melt, the larger olivines should have settled faster than the smaller but more dense chromites. The modal grading, therefore, appears to be upside down. Jackson (1961) concluded from this and other observations that in situ bottom crystallization, not gravitational settling, created this layering. Kinetic factors may also play a role in development of modal layering (Section 7.9.2; Figure 7.46).

Evidence for upward migration of melt through the cumulus floor pile can be seen in mineral compositions in the Muskox intrusion (Figure 12.17). This layered intrusion, like the Stillwater, Duluth, Bushveld, and Great Dyke intrusions (Table 12.5), formed from episodic replenishment of basaltic magma during its crystallization. This open-system recharge is usually evident in upward reversals in compositional variation (Figure 12.18) and is logical in view of the multiple basalt dikes, sills, and lava flows spatially and temporally associated with the intrusions. Discontinuities in the chemical composition of cumulus chromite and olivine occur *up section* from the modal break marking

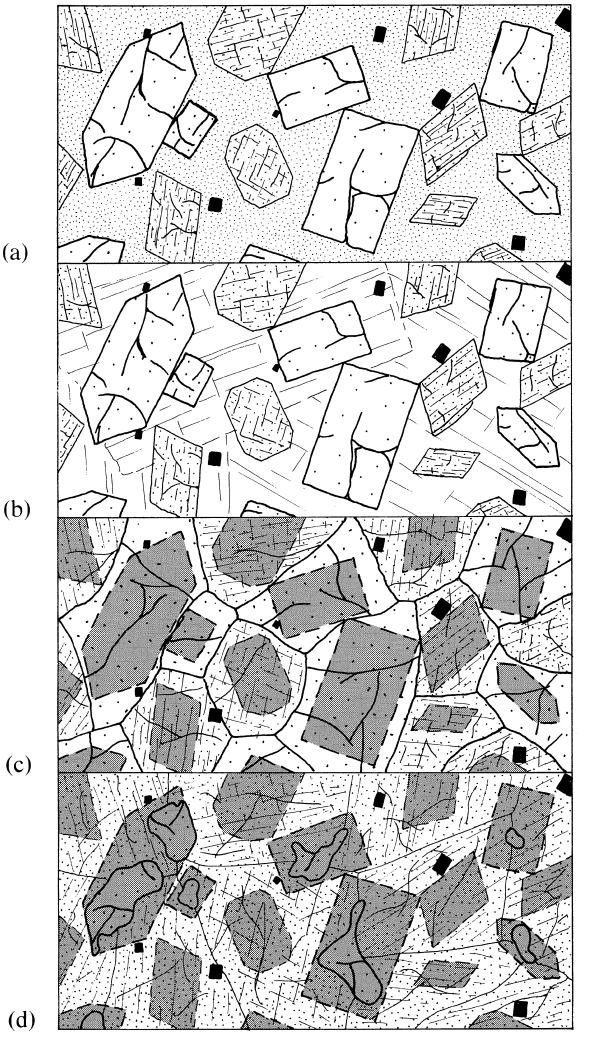


**12.16** Evolution of **cumulus** fabric. The three **postcumulus** processes illustrated in (b–d) are ideal end members; real **cumulate rocks** generally form by some combination of these processes. See Hunter (1996) and Morse (1998) for additional discussion of cumulus textures. (a) Original cumulus grains of olivine (bold relief), pyroxene (with cleavage), and chromite (small black) in a melt (stippled). (b) Postcumulus **cementation** and development of poikilitic texture. The intercumulus melt surrounding the cumulus grains in (a) crystallized as large plagioclase grains, filling the intercumulate pore volume. Extraneous ions in the melt (Fe, Mg, Ti, etc.) not required by the growing plagioclase must be transferrred out of this space, perhaps by ionic diffusion. (c) Postcumulus **overgrowth** and development of equilibrated texture with approximately 120° triple-grain-boundary junctions. Intercumulus melt surrounding the cumulus grains (shaded areas enclosed by dashed outlines) in (a) crystallized as secondary enlargements on the cumulus olivines and pyroxenes until all pore space was eliminated. Plagioclase either was unstable or did not nucleate. Monomineralic dunites, pyroxenites, and anorthosites can originate by secondary enlargement of accumulations of olivines, pyroxenes, and plagioclases, respectively. Ions not needed during enlargement are transferred out of the local interstitial volume by some means. (d) Postcumulus **reaction replacement** combined with overgrowth. Intercumulus melt reacted with cumulus grains (shaded areas enclosed by dashed outlines) in (a), partly consuming olivines. Simultaneous secondary enlargement of the cumulus pyroxenes eliminated all pore spaces.

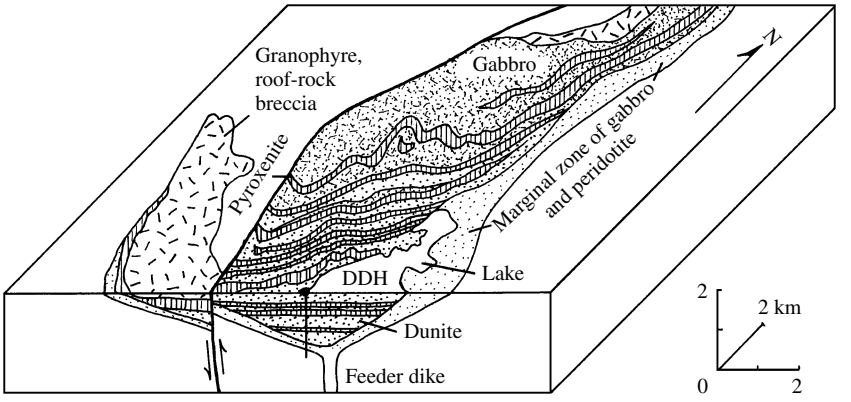


**12.17** Schematic block diagram of the central segment of the Muskox layered intrusion, Northwest Territories, Canada. Regional tilting to the north of about 5° exposes most of this 1270-Ma trough-shaped intrusion. Feeder dike 150–500 m wide of picrite and gabbro extends tens of kilometers southward. The intrusion is as much as 11 km wide and at least 150 km long before disappearing under covering roof rock. Above the troughlike marginal zone of gabbro and peridotite is a 1800-m-thick series of 42 mappable layers individually ranging in thickness from 3 to 350 m that are predominantly dunite with a lesser proportion of pyroxenite. This layered series is overlain by gabbro and then granophyre formed from the evolved residual magma. DDH, diamond drill hole, whose core has been investigated in detail (Figure 12.18). (Redrawn from Irvine, 1980.)

the cyclic unit boundary. Irvine (1980) explains this discrepancy between modal and chemical breaks on the basis of compaction of the cumulate pile and upward transfer of the intercumulus melt out of it. Migration of melts having lower Mg/(Mg + Fe) and Ni/(Ni + Mg + Fe) ratios from the underlying cumulate unit into the overlying cumulus olivines and chromites causes them to reequilibrate via reaction relations. The wave of reequilibration for Mg and Fe extends farther into the overlying cyclic unit than does that of Ni because the melt contains about a third as much Mg + Fe as the cumulus crystals but only about a tenth as much Ni. Accordingly, adjustments in Mg and Fe are more pronounced.

In large, slowly cooled intrusions, a substantial fraction of the intercumulus melt can be transferred via filter pressing or convective melt fractionation from the compacting floor cumulates back into the uncrystallized central part of the intrusion. This is an effective crystal-melt fractionation that has in the past been attributed to crystal settling through the whole chamber.

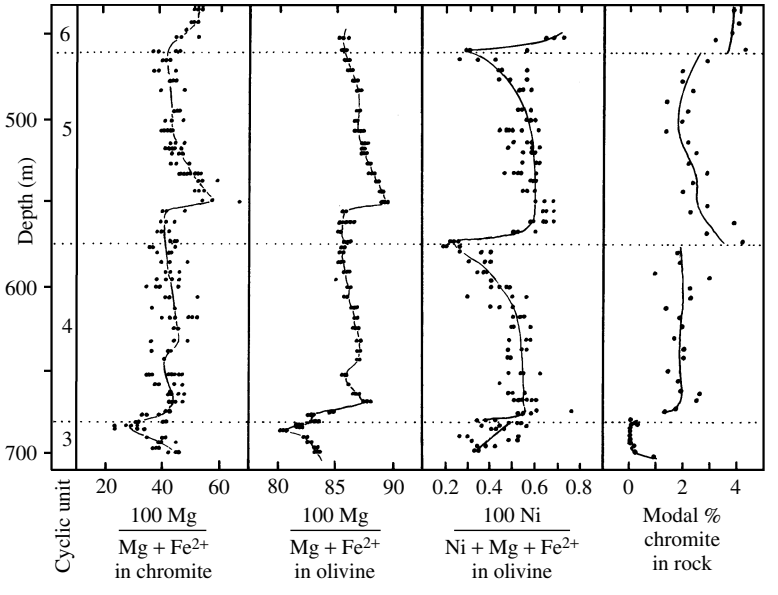


**12.18** Analytical data on a part of the core from a drill hole into the Muskox intrusion (DDH in Figure 12.17). Boundaries of a cyclic unit are defined by discontinuities in modal proportion of cumulus chromite grains in right-hand panel. In the Muskox, each of the 25 cyclic units represents a magma recharge into the intrusion. Discontinuities in chemical composition of cumulus olivine and chromite occur above the modal boundaries. The top of unit 3 is chromite-free olivine clinopyroxenite; all other rock is chromite-bearing dunite. (Redrawn from Irvine, 1980.)

Skaergaard Intrusion. No discussion of layered intrusions would be complete without mention of the intensely studied Skaergaard intrusion, located in the remote southeast coast of Greenland just above the Arctic Circle. This intrusion and related dikes and overlying thick lava flows formed during the early Tertiary opening of the north Atlantic (see Figure 13.23). Ironically, the more that has been learned, from the earliest studies by Wager and Deer (1939) to later studies by A. R. McBirney and associates (e.g., 1996), the more controversy seems to develop (Irvine et al., 1998).

In contrast to many large differentiated sills and larger intrusions, the exposed part of the Skaergaard intrusion (Figures 12.19 and 12.20) reveals no unequivocal indication of multiple injections of magma that mixed with previously fractionated magma. For example, compatible element trends, such as for Ni, are continuous without major breaks (Figure 12.20). Therefore, the exposed part of the Skaergaard—above a hypothetical Hidden Zone—may have formed by fractionation in a closed magma system. Unfortunately, no unaltered "chilled" margin rock has been found that might represent the pristine, parent magma from which the intrusion fractionated.

Crystallization in the Skaergaard was dominantly upward from the floor, producing an uncertain amount of the Hidden Zone plus the exposed Layered Series of about 2500 m. This is much greater than the thickness of the downward crystallized Upper Border Series. These two series meet at the Sandwich Horizon, which represents the last-crystallized part of the intrusion, and are enveloped within the still thinner Marginal Border Series, the part of the intrusion solidifying inward from the sidewalls. That this is indeed the pattern of inward crystallization of the intrusion is shown by variations in whole-rock chemical and mineral compositions and phase layering. **Phase layering** is the abrupt appearance or disappearance of a particular mineral, such as the vertical disappearance of olivine defining the lower boundary of the Middle Zone of the Layered Series and its reappearance in the Upper Border Series. **Cryptic layering** reflects systematic changes in the chemical composition of cumulus minerals, shown in the middle panel of Figure 12.20. Plagioclase becomes more sodic, to $An_{25}$ in the Sandwich Horizon, from as much as $An_{69}$ in the uppermost part of the intrusion and $An_{66}$ in the lowest exposed part. Olivine ranges from $Fo_{68}$ to pure fayalite $Fo_0$ and clinopyroxene to Mg-free hedenbergite in the Sandwich Horizon. These cryptic variations are more or less symmetric inward to the Sandwich Horizon, as are whole-rock chemical compositions (Figure 12.21).

The extreme enrichment in Fe and limited late enrichment in silica and alkalies have made the **Skaergaard trend** a reference standard for fractionation of tholeiitic basalt magma (Table 12.6; Figures 12.21 and 12.22). However, the physical mechanism of fractionation that operated in the Skaergaard is still controversial. Two competing hypotheses are briefly summarized in the following two paragraphs (see also Special Interest Box 8.1). The debate is yet another example that experienced petrologists can arrive at markedly contrasting opinions about the same rock.

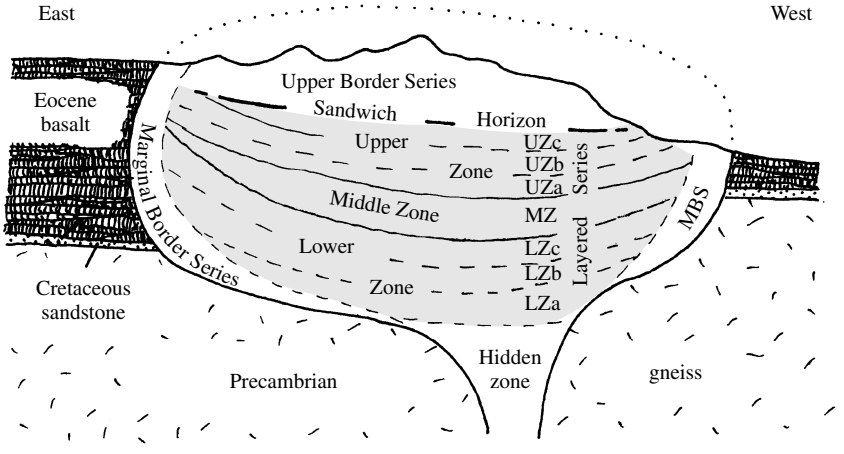


**12.19** Schematic cross section through the Skaergaard intrusion, Greenland. Emplaced at 55.7 Ma, the intrusion measures about 6 × 11 km on the ground and, because of a regional northward tilt of 15°–25°, the 1200 m of glacially carved topographic relief exposes an almost continuous 3500-m stratigraphic section through the body. Configuration of the deeper unexposed part of the intrusion, the Hidden Zone, is based on geophysical measurements. The intrusion can be conveniently divided into four parts (see also Figure 12.20): (1) Marginal Border Series (MBS) consisting of an inner Layered Series and an outer Tranquil Zone; (2) Thick Layered Series (shaded), consisting, in ascending order, of the Lower Zone, which is divided into three parts (LZa, LZb, LZc); the Middle Zone (MZ); and the Upper Zone, which is divided into three parts (UZa, UZb, UZc); (3) Upper Border Series (UBS); (4) last crystallizing Sandwich Horizon. (Redrawn from McBirney, 1993.)

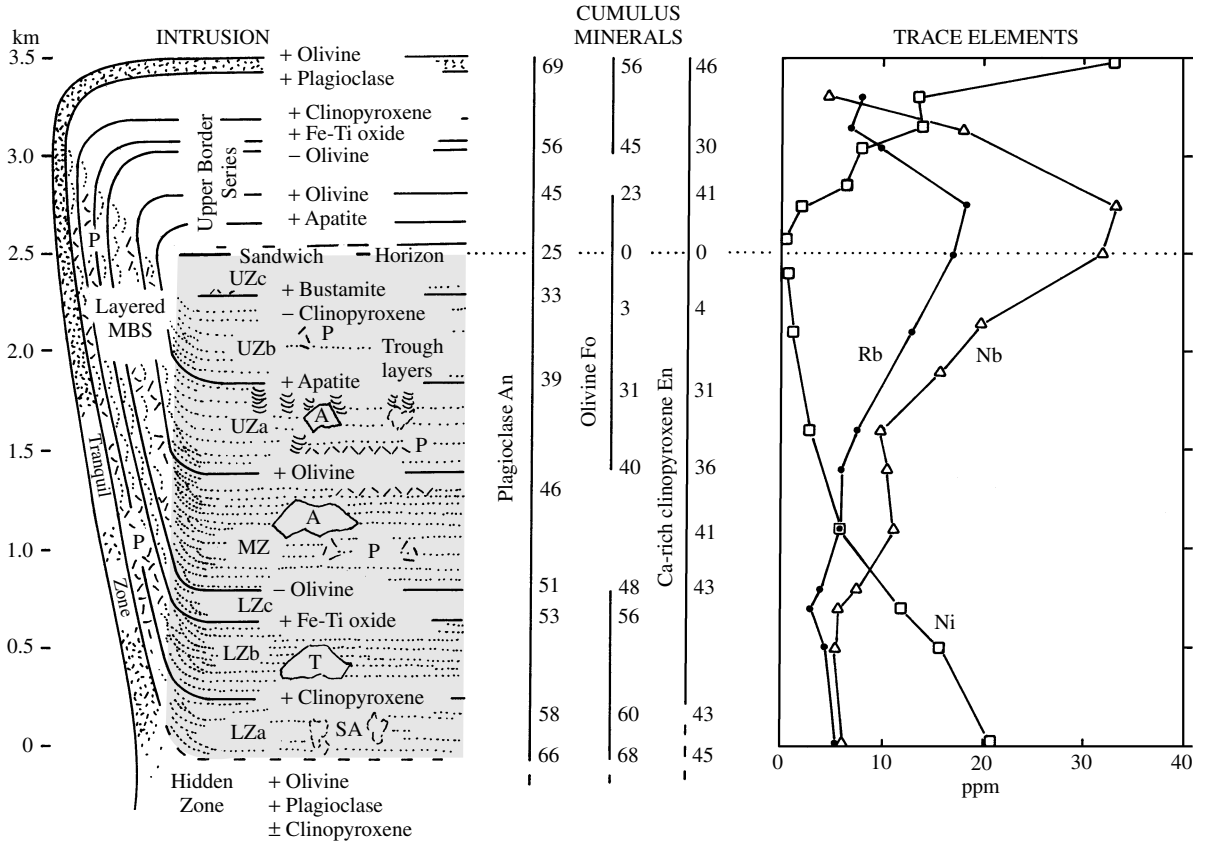


**12.20** Compositional relations and layering in the Skaergaard intrusion. Left-hand panel is a more detailed diagram of Figure 12.19 indicating **phase layering,** which delineates the successive layer units (e.g., LZb, LZc, MZ). Also indicated are correlations of crystallization stages in the Layered, Marginal Border, and Upper Border Series. For example, after early crystallization of the texturally isotropic Tranquil Zone against the wall rock, an upper layer of the Upper Border Series crystallized concurrently with an outer layer of the Marginal Border Series (MBS) and the lowermost layer of the Layered Series, LZa. Modal graded layering is represented schematically by dotted lines. Note cross-bedding in modal layers at the junction of the subhorizontal Layered Series and the steeply inclined Marginal Border Series and trough layers in the UZa layer. P, schematically indicated patchy and strata-bound masses of coarse-grained mafic pegmatite; SA, schematically indicated masses of secondary anorthosite; T and A, respectively, schematically indicated blocks of troctolite (olivine + plagioclase rock) and anorthosite stoped off the roof of the intrusion. There are many more of SA, T, and A than shown. (Redrawn from McBirney, 1996; Irvine et al., 1998.)

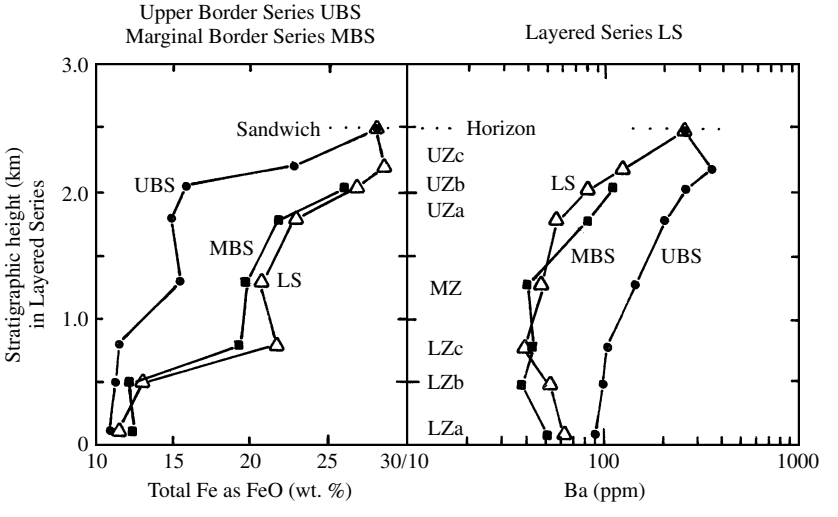


**12.21** Chemical variations in the Skaergaard intrusion. Elements in the Upper Border Series and Marginal Border Series are plotted with respect to equivalent unit in Layered Series. (Redrawn from McBirney, 1996.)

**Table 12.6.** Average Compositions of the Units in the Layered Series, Sandwich Horizon (SH), and Granophyre, Skaergaard Intrusion

| | LZA | LZB | LZC | MZ | UZA | UZB | UZC | SH | GRANO |
|---|---|---|---|---|---|---|---|---|---|
| $SiO_2$ | 48.12 | 48.84 | 41.10 | 42.79 | 43.07 | 41.78 | 46.00 | 49.43 | 60.23 |
| $TiO_2$ | 1.35 | 1.44 | 6.92 | 6.79 | 5.67 | 4.06 | 2.63 | 2.23 | 1.18 |
| $Al_2O_3$ | 16.81 | 12.55 | 11.02 | 11.53 | 11.17 | 9.51 | 7.86 | 7.93 | 11.29 |
| FeOt | 11.13 | 12.84 | 21.10 | 20.00 | 22.52 | 26.64 | 28.67 | 27.87 | 14.08 |
| MnO | 0.16 | 0.21 | 0.26 | 0.26 | 0.31 | 0.41 | 0.65 | 0.25 | 0.24 |
| MgO | 9.42 | 10.13 | 7.61 | 6.24 | 5.62 | 3.41 | 0.38 | 0.09 | 0.51 |
| CaO | 10.11 | 11.57 | 9.77 | 9.87 | 8.62 | 9.36 | 10.14 | 8.23 | 5.11 |
| $Na_2O$ | 2.52 | 2.13 | 1.97 | 2.23 | 2.55 | 2.59 | 2.42 | 2.72 | 3.92 |
| $K_2O$ | 0.27 | 0.20 | 0.20 | 0.21 | 0.26 | 0.36 | 0.41 | 0.72 | 1.94 |
| $P_2O_5$ | 0.11 | 0.09 | 0.05 | 0.08 | 0.22 | 1.88 | 0.84 | 0.53 | 0.27 |
| Sr | 285 | 219 | 199 | 218 | 233 | 244 | 263 | 450 | |
| Zr | 93 | 81 | 72 | 80 | 95 | 97 | 135 | 324 | |
| La | 5.62 | 4.68 | 3.84 | 3.09 | 3.49 | 14.57 | 22.68 | 57.8 | |
| Sm | 2.47 | 3.08 | 2.34 | 2.10 | 2.10 | 10.00 | 15.27 | 34.5 | |

Total oxides are 100.00.
Data from McBirney (1996).

In their classic study, Wager and Deer (1939) postulated that convection currents were responsible for the rhythmic modal layering, trough layering, igneous lamination, and local lenticular and cross bedding and slump structures. They envisaged the Layered Series as having formed by gravitational settling and sorting of crystals from convection currents that descended from the walls and swept inward across the cumulate floor. Depending on the vigor of convection, modally graded layers would be thin or thick or rhythmic. Irvine et al. (1998) reaffirmed and refined the convection-driven sedimentation hypothesis, documenting in considerable detail what they believe to be supporting evidence.

Beginning in the late 1970s, **magmatic sedimentation** via convection in the Skaergaard was rejected by McBirney and coworkers (1996), largely because plagioclases dominating the cumulate fabric should have floated, not sunk, in the increasingly denser Fe-rich melts. They appealed, instead, to fractional crystallization driven by compaction and convective melt fractionation within the pile of cumulate crystals on the intrusion floor. Because this fractionation is driven by gravity, there ought to be different fractionation effects in the Layered Series that accumulated on the floor versus in the Upper Border Series that was created near the roof. And both might differ from the Marginal Border Series. Figure 12.21 shows such differences. Upper Border Series rocks are depleted in Fe relative to Layered Series rocks because negatively buoyant Fe-rich residual melts, perhaps carrying some suspended crystals, drained out of the roof region and ponded in floor cumulates. Marginal Border Series rocks are slightly less Fe-rich than Layered Series rocks, again reflecting draining out of Fe-rich melts, but not as efficiently as from the roof. The greater concentration of incompatible elements, such as Ba, in Upper Border Series rocks than in Layered Series is thought to reflect even later-stage, postpeak Fe-enrichment infiltration of buoyant incompatible-element-enriched residual melts derived from underlying magma. These late buoyant melts were relatively enriched in silica and alkalies and crystallized largely as scattered patches and dikes of granophyric rock throughout the intrusion but especially in the Upper Border Series. Some late mafic granophyres may have formed from immiscible melts. Other granophyres may be fused blocks of quartzofeldspathic gneiss country rock.

Magmatic Replacement in Large Layered Intrusions. Meter-scale, patchy masses of rock in the Skaergaard and other intrusions appear to have formed by replacement of original rock, facilitated by local concentrations of water. These masses include secondary anorthosite and mafic pegmatite that are commonly adjacent to one another (SA and P, respectively, in the left panel of Figure 12.20). The origin of the anorthosite (>90% plagioclase) by secondary, volume-for-volume metasomatic replacement is indicated by undisturbed continuity of layering from adjacent rock through the anorthosite. Irvine et al. (1998) suggest that locally higher concentrations of water in the intercumulus melt shift the olivine-pyroxene-plagioclase cotectic toward plagioclase, locally precipitating more of this phase and displacing mafic minerals into peripheral areas. Unusually coarse-textured gabbroic rock, or mafic pegmatite, some having additional biotite and amphi-

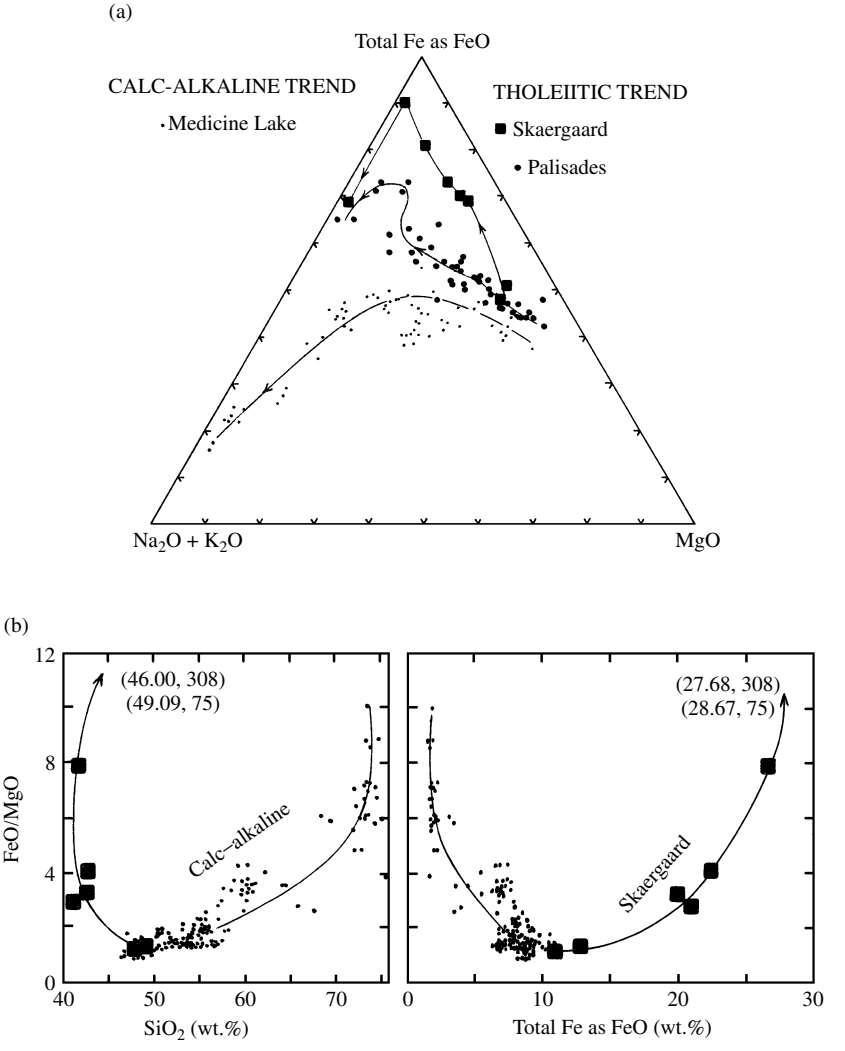


**12.22** Comparison of tholeiitic and calc-alkaline differentiation trends. (a) Data points are rocks from the Skaergaard intrusion (data from McBirney, 1996; see also Table 12.6), the Palisades sill (data from Shirley, 1987), and the Medicine Lake volcanic field (data from Grove and Baker, 1984). (b) Palisades rocks are not plotted. The line with arrow through the Skaergaard rocks points in direction of more evolved rocks, the two most Fe-rich lying off the diagram at the indicated coordinates.

bole that are absent generally from the cumulates, is believed to have crystallized from locally more hydrous and buoyant intercumulus melts rising diapirically through the cumulus pile. The source of the water may be the intercumulus melt itself or perhaps water absorbed from country rock.

The origin of widespread thick layers of anorthosite in some layered intrusions, as much as 600 m in the Stillwater, is unresolved but cannot be due to secondary processes.

Meter-thick layers ("reefs") of pegmatitic pyroxenite in the Bushveld and Stillwater are major world repositories of platinum-group elements (PGEs), consisting of Pt, Pd, Rh, Ir, Ru, and Os. The traditional view has been that the PGE-bearing minerals were concentrated as dense immiscible sulfide melts on the intrusion floor. However, the intimate association of the PGE minerals with pegmatite and hydrous minerals as well as exceptionally high concentrations of rare earth elements (REEs) in pyroxenes are interpreted in terms of redistribution of interstitial melt driven by compaction of the cumulate layers (Mathez et al., 1997).

### 12.4.3 Oceanic-Ridge Magma Chambers

After polybaric fractionation of olivine during their ascent from the mantle source, primary mid–ocean ridge basalt **(MORB)** magmas experience further differentiation at low *P* in crustal storage chambers beneath the rift.

Intuitively, it seems unlikely that the crustal chambers filled with magma would remain perfectly closed systems throughout their entire history of solidification. In the actively spreading rift environment, fresh

draughts of more primitive magma would be expected to be episodically injected into the chamber of fractionating magma from the underlying mantle source (Figure 12.12). Three lines of evidence were found by early investigators (e.g., Rhodes et al., 1979) indicating chamber replenishment and mixing:

1. Disequilibrium phenocryst-melt compositions and textures: Many larger olivines and especially plagioclases have corroded, spongy cores ($Fo_{85–90}$ and $An_{83–86}$) that are surrounded by more evolved crystalline material.
2. Glass inclusions within the high-*T* cores have compositions similar to the most primitive MORB and unlike the glass in the surrounding matrix.
3. Element variation trends follow those anticipated by fractionation of major phenocrystic phases combined with mixing of replenishing draughts of primitive magma (Figures 12.23–12.25).

Thus, the limited compositional variation in most MORBs reflects recurring replenishment and mixing of relatively primitive mantle-derived magmas with fractionating magma in rift chambers, moderating the effects of crystal-melt fractionation.

However, less common seafloor basalts found locally along the Galapagos rift and other sites on the East Pacific Rise follow a tholeiitic fractionation trend of extreme Fe-enrichment and limited enrichment in silica and alkalies resembling the Skaergaard trend (Figure 12.22). Apparently, in local more closed-system chambers, 60–80% fractionation of olivine, plagioclase, and lesser clinopyroxene produces ferrobasalts (13–16 wt.% total Fe as FeO) and less common ferrodacites (5–11 wt.% FeO, 64–71 wt.% $SiO_2$).

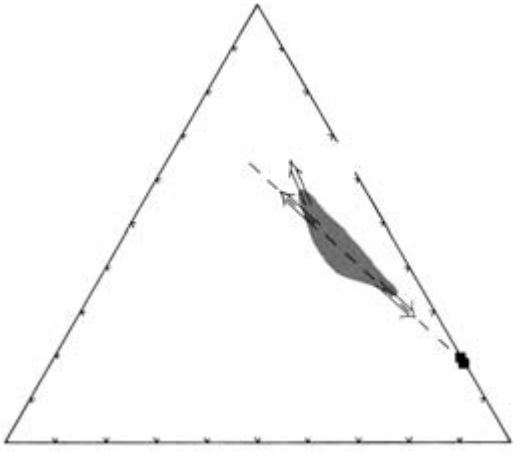

**12.23** Crystal-melt fractionation in MORB magmas. Analyzed glasses from Bryan and Moore (1977) plot in shaded area. Filled squares are analyzed olivine (Ol) phenocrysts and dashed line is olivine control line. Accumulation or subtraction of olivine produces most of the compositional variation in the glasses, whereas limited fractionation of plagioclase (Pl) and pyroxene (Px) from low-MgO magmas shifts the trend slightly toward more FeO-rich compositions.

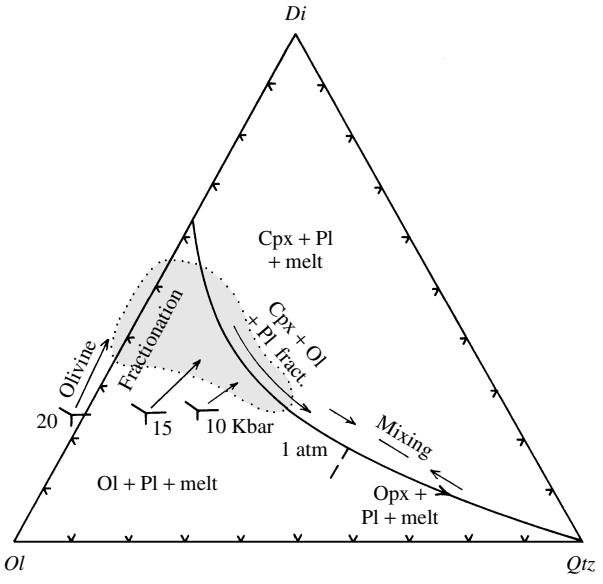


**12.24** Compositional relations in seafloor basalts plotted in terms of normative *Di, Ol,* and *Q*. Plagioclase and/or spinel is stable in all assemblages. Experimentally determined beginning-of-melting invariant points in peridotite source rock at 20, 15, and 10 kbar, and 1 atm. Curved boundary line on 1 atm liquidus. Shaded area encompasses nearly 2000 analyses of basalts that are interpreted to have formed by polybaric fractionation of olivine from primary melts generated at 10–20 kbar. Subsequent low-*P* fractionation of plagioclase, clinopyroxene, and olivine from these primitive parent magmas within crustal magma chambers yields evolved magmas extending down the boundary line. Many of these derivative magmas have been modified by mixing with more silica-rich magmas. Significant enrichment in Fe in derivative magmas cannot be represented in this diagram. (Redrawn from Natland, 1991.)

## ❊12.5 ORIGIN OF THE CALC-ALKALINE DIFFERENTIATION TREND

Several variation diagrams have been employed to distinguish between the **tholeiitic differentiation trend** of Fe enrichment with limited felsic derivatives and the **calc-alkaline trend** of limited Fe enrichment and abundant felsic derivatives (Figures 2.17 and 12.22; see also Miyashiro, 1974). The tholeiitic rock suite is typical of differentiated basaltic intrusions, as just described, as well as island arcs, whereas the calc-alkaline suite is typical of continental margin arcs.

These contrasting rock suites and their associated magmatic differentiation trends have been recognized, and their origin debated, for many decades. Prior to the mid-twentieth century, C. N. Fenner believed that crystallizing basaltic magmas evolved along a trend of Fe enrichment at nearly constant silica concentration,

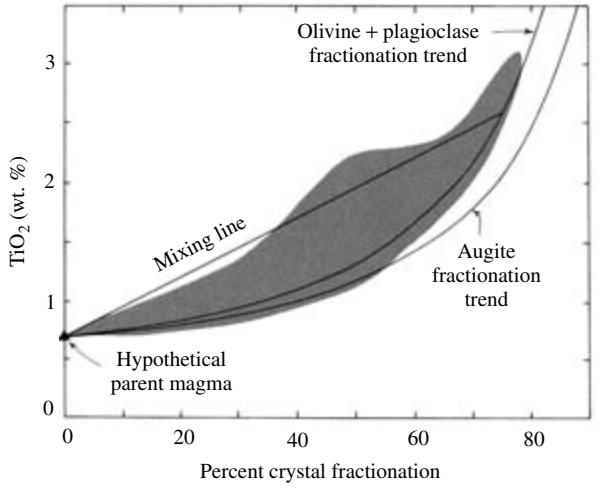


**12.25** Effects of crystal-melt fractionation and magma recharge and mixing on the $TiO_2$ content of seafloor basalts. A hypothetical parent magma having 49.9 wt.% $SiO_2$ and 0.7 wt.% $TiO_2$ from which olivine, plagioclase, and augite of realistic compositions are fractionated produces residual melts along the curved fractionation-trend lines. Intermittent mixing of such residual melts with additional draughts of parental magma would produce magmas whose compositions lie within the shaded lens-shaped area bounded by the mixing line and the curved fractionation trend lines. The shaded area represents over 600 chemically analyzed seafloor glasses. (Redrawn from Rhodes et al., 1979.)

now designated the tholeiitic trend and exemplified by the extreme Fe enrichment of the Skaergaard intrusion. On the other hand, N. L. Bowen advocated a trend of limited Fe enrichment and greater production of felsic end products, exemplified by calc-alkaline rocks. It is now realized that there is a range of differentiation processes that can operate on primitive basaltic magmas, producing a continuous spectrum of rock suites and trends whose end members are the Skaergaard and the calc-alkaline trends. It should be recalled that this continuum and its two end members constitute the subalkaline suite (Section 2.4.5), which accounts for about 90% of global magmatism (Figure 1.1); hence, contrasts in the evolution of tholeiitic and calc-alkaline magmas merit special attention.

### 12.5.1 Tonga–Kermadec–New Zealand Arc

This continuous arc in the southwest Pacific Ocean developed above the subducting Pacific oceanic plate during the late Cenozoic; the volcanic rocks in the arc provide one of the clearest examples of contrasting tholeiitic and calc-alkaline suites or trends (Figures 2.17 and 2.18). Tholeiitic rocks in the youthful Tonga-Kermadec arc rest on oceanic crust, whereas calc-alkaline rocks in the along-strike Taupo volcanic zone of the North Island of New Zealand rest on continental crust (Figure 12.26). New Zealand obviously harbors a greater volume of silicic rocks than mafic-intermediate composition rocks, whereas the reverse is true of the oceanic Tonga-Kermadec part of the arc. Relatively primitive basalts in the two arc segments have similar trace element concentrations and patterns, suggesting a similar ancestry in the subarc mantle wedge. However, the Taupo basalts have more radiogenic Nd and Sr isotopic ratios that are consistent with assimilation of an older sedimentary component resembling metamorphosed Mesozoic sedimentary rocks exposed to the east of the volcanic zone.

If the 16,000 $km^3$ of extruded rhyolite magma in the Taupo volcanic zone originated wholly by fractionation of parental basalt magma, about 10 times as much basalt magma would have been required. This questionable volume plus the relative minor amounts of contemporaneous intermediate andesite and dacite make such an origin unlikely. On the other hand, the high crustal heat flow and intense geothermal activity associated with the voluminous rhyolite volcanism suggest a major heat source in the crust; this is speculated to be underplated basalt magma from the mantle wedge. Compared to fractionation origin, rhyolite magma generation by partial melting of older continental rocks requires a significantly smaller mass of basalt magma, approximately equal to that of the lower crustal rocks being melted (Section 11.1.1). That the erupted basaltic magmas in the Taupo zone appear to show crustal contamination supports the hypothesized model.

### 12.5.2 Factors Controlling Development of the Calc-Alkaline Trend

Water is an essential component in arc magma generation, evolution, and typical explosive behavior. Water promotes partial melting in the hydrated mantle wedge overlying subducting wet oceanic crust. Subsequently, these hydrous primitive magmas evolve along distinct trends. High water fugacities stabilize amphiboles and biotite and depolymerize the melt, expanding the stability field of olivine while restricting plagioclase. Enhanced olivine crystallization reduces Mg, Fe, Ni, and Cr concentrations in residual melts. Restriction of plagioclase precipitation to calcic compositions, $An_{70-90+}$, enriches residual melts in Na and K. These factors are some of those responsible for development of the felsic calc-alkaline trend, rather than the Skaergaard trend of increasing Fe.

In continental arcs, at least three possible factors, not present in island arcs, might modify primitive magmas derived from the mantle wedge, producing greater proportions of felsic calc-alkaline rocks:

1. Sediment eroded off a high mountain terrain and deposited in the adjacent ocean trench, as well as tectonic slices carved off the edge of the overriding plate, may be subducted with the oceanic crust. This continental material may be partially melted,

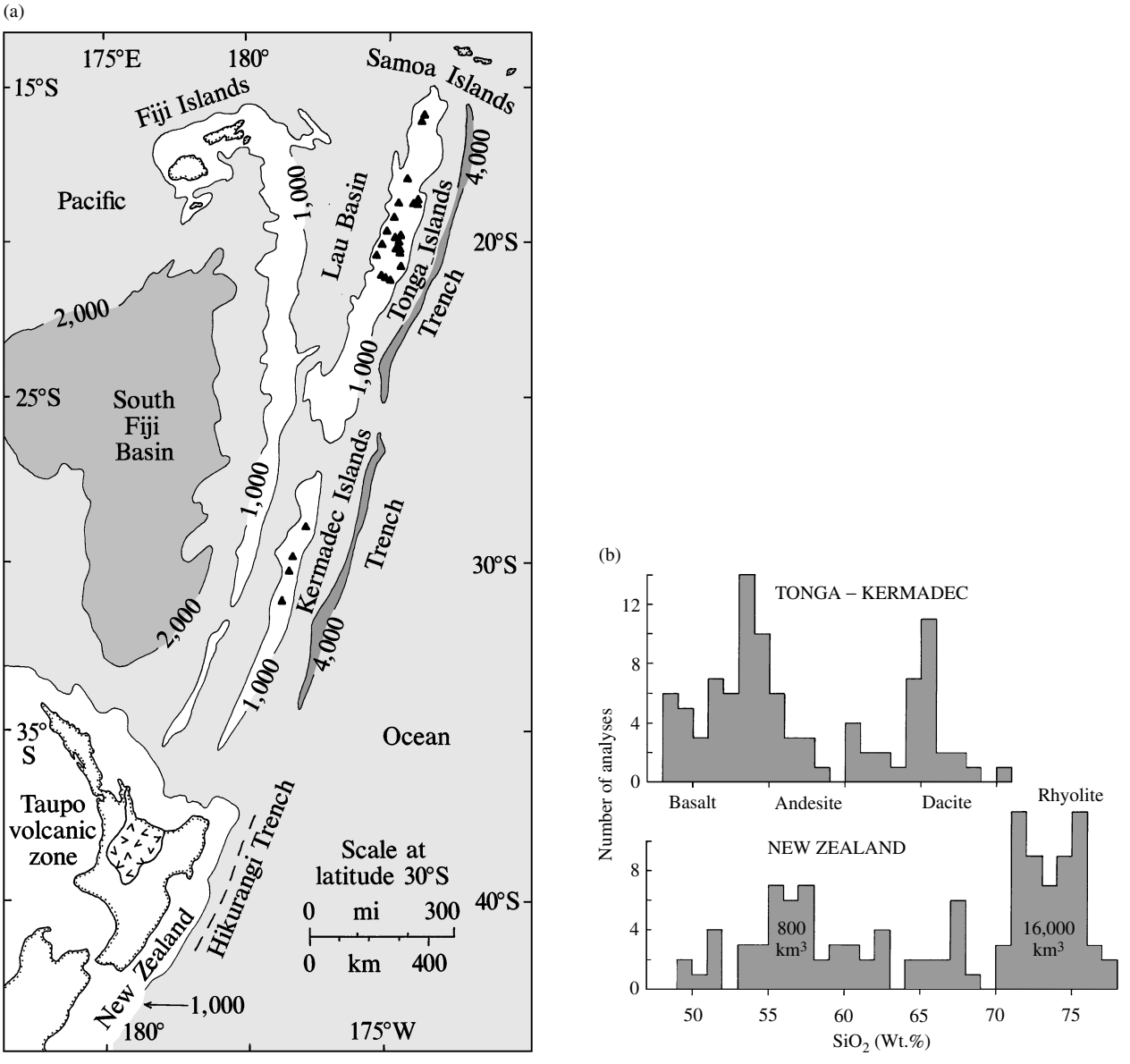


**12.26** Tonga–Kermadec–New Zealand volcanic arc and arc rocks in the southwestern Pacific. (a) Volcanic islands indicated by filled triangles. Bathymetric contours are in fathoms (1 fathom = 1.83 m). For a more detailed, larger-scale map of the North Island of New Zealand see Figure 13.27. (b) Frequency distribution of silica in analyzed rocks from the Tonga-Kermadec island arc and from the North Island of New Zealand. Tonga is chiefly basalt and andesite; sparse dacite is overrepresented. In New Zealand, rhyolite is estimated to be about 20 times more voluminous than andesite. (Redrawn from Ewart et al., 1977.)

enhancing production of felsic magmas in the subarc environment.

2. Subcontinental lithospheric mantle may have been static (nonconvecting) and metasomatically enriched over long periods; ascending magmas scavenge these enrichments.
3. Contributions from the continental felsic crust itself are probably important. Where the continental crust is thicker there is a tendency for a greater proportion of $K_2O$ at a given $SiO_2$ content, greater proportion of felsic rock types (dacite and rhyolite), and higher proportion of $K_2O/Na_2O$ in andesite (Figure 12.27); these compositional parameters indicate that the longer the path through which magmas rise in their journey to the surface of the continental crust the more they take on felsic continental characteristics. The first factor listed is independent of the path length and, thus, probably less significant. The "scatter" in the global data of Figure 12.27 likely reflects the compositional heterogeneity of the continental crust and other irregularities in differentiation processes.

The greater the path length that ascending magmas take through the continental crust the greater the op-

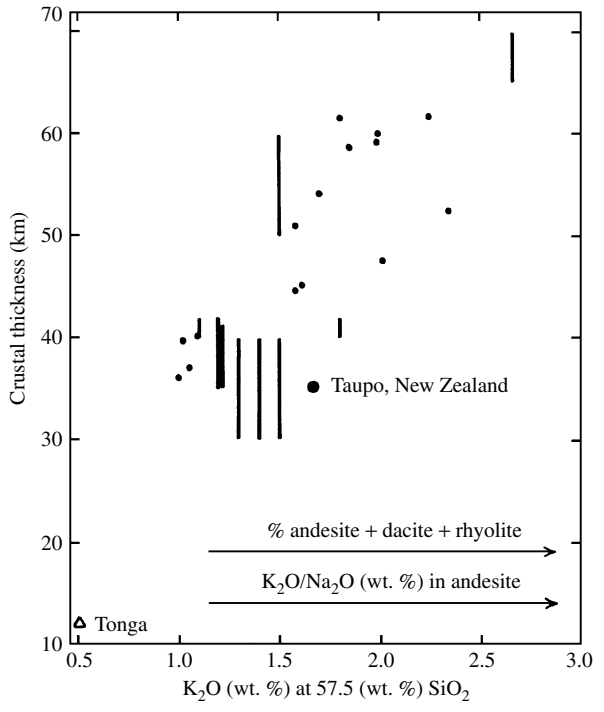


**12.27** Correlation between thickness of continental crust (>30 km) and compositional parameters. The graphed parameter is the concentration of $K_2O$ at 57.5 wt.% $SiO_2$ from a best-fit line through a $K_2O$ versus $SiO_2$ wt.% variation diagram for a rock suite; for example, values of $K_2O$ at 57.5 wt.% $SiO_2$ for the New Zealand suite and, for comparison, the Tonga suite are taken from Figure 2.18. Bars in diagram indicate variable crustal thickness for the $K_2O$ value. Two other parameters not graphed also show a positive correlation with crustal thickness; these are the $K_2O/Na_2O$ in andesite (57–63 wt.% $SiO_2$) and the proportion of andesite + dacite + rhyolite to basalt. (Data from Leeman, 1983; Hildreth and Moorbath, 1988.)

portunity for assimilation and fractional crystallization to produce felsic calc-alkaline magmas. Mantle-derived basaltic magmas intruded in the lower crust can assimilate felsic rock and mix with silicic partial melts generated by the heat from the crystallizing and usually fractionating basalt magma. The combined effects of simultaneous assimilation and fractional crystallization **(AFC)** on evolving magma systems were first formalized by Taylor (1980) and further quantified by De Paolo (1985) and Aitcheson and Forrest (1994). Their equations express isotopic ratios and element concentrations of hybrid daughter magmas to be expected from an assumed contaminant and parent magma based on the following:

1. Estimated bulk distribution coefficients
2. Ratio of the rates of assimilation to fractional crystallization
3. Remaining melt fraction
4. Effects of magma recharge and eruption

The first three parameters are commonly chosen to provide the best fit to the analytical data (Figure 12.28). This AFC model works best in cases in which the contaminant and parent magma compositions differ significantly.

The basalt-andesite-dacite-rhyolite suite in the Medicine Lake volcano in the northern California Cascade volcanic belt (Grove and Baker, 1984) is typical of many calc-alkaline suites. A general trend of increasing $^{87}Sr/^{86}Sr$ with increasing silica is consistent with progressive assimilation of felsic crust in mantle-derived magmas. Elevated incompatible element (e.g., Rb) concentrations in some evolved rocks indicate that fractional crystallization alone cannot be responsible, but combined fractionation and assimilation of felsic rocks can (Figure 12.29a). Mixing of basaltic and rhyolitic magmas also seems required for some rock types and is supported by mingled dacite and rhyolite lavas and by disequilibrium phenocryst assemblages in basaltic andesites and dacites; these assemblages include, in a single sample, Mg-rich olivine ($Fo_{90}$), calcic plagioclase ($An_{85}$), reversely zoned orthopyroxene with Fe-rich cores and Mg-rich rims, and reversely zoned plagioclase with andesine cores and labradorite

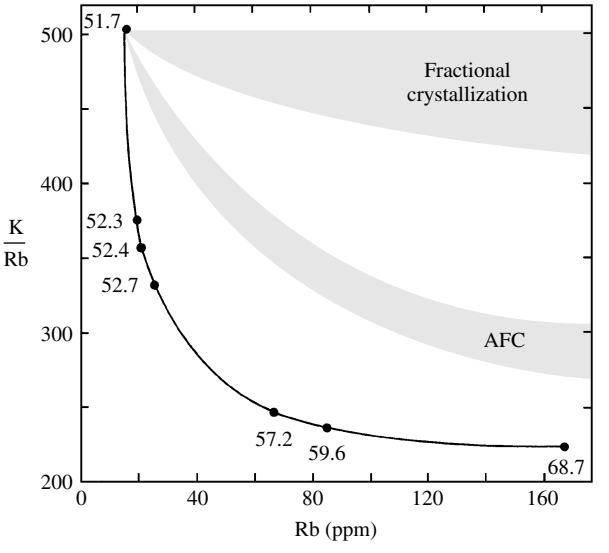


**12.28** K/Rb versus Rb in the Volcanes Planchon-Peteroa-Azufre at 35°15′S latitude in the central Andes. Numbers alongside solid circles are weight percentage silica in rock samples that range from basalt to dacite. *For reference only* are approximate trends to be expected (1) if a parent magma, represented by the rock that has 51.7 $SiO_2$, were to evolve wholly by fractional crystallization of olivine, pyroxene, and plagioclase or (2) if fractional crystallization acted in concert with assimilation of granite (AFC). Note that fractional crystallization alone is inadequate to account for these diverse evolved rocks because of the similarity in partition coefficients of K and Rb. In contrast, assimilation of granite country rocks in concert with fractional crystallization is a more viable diversification process. (Redrawn from Hildreth and Moorbath, 1988.)

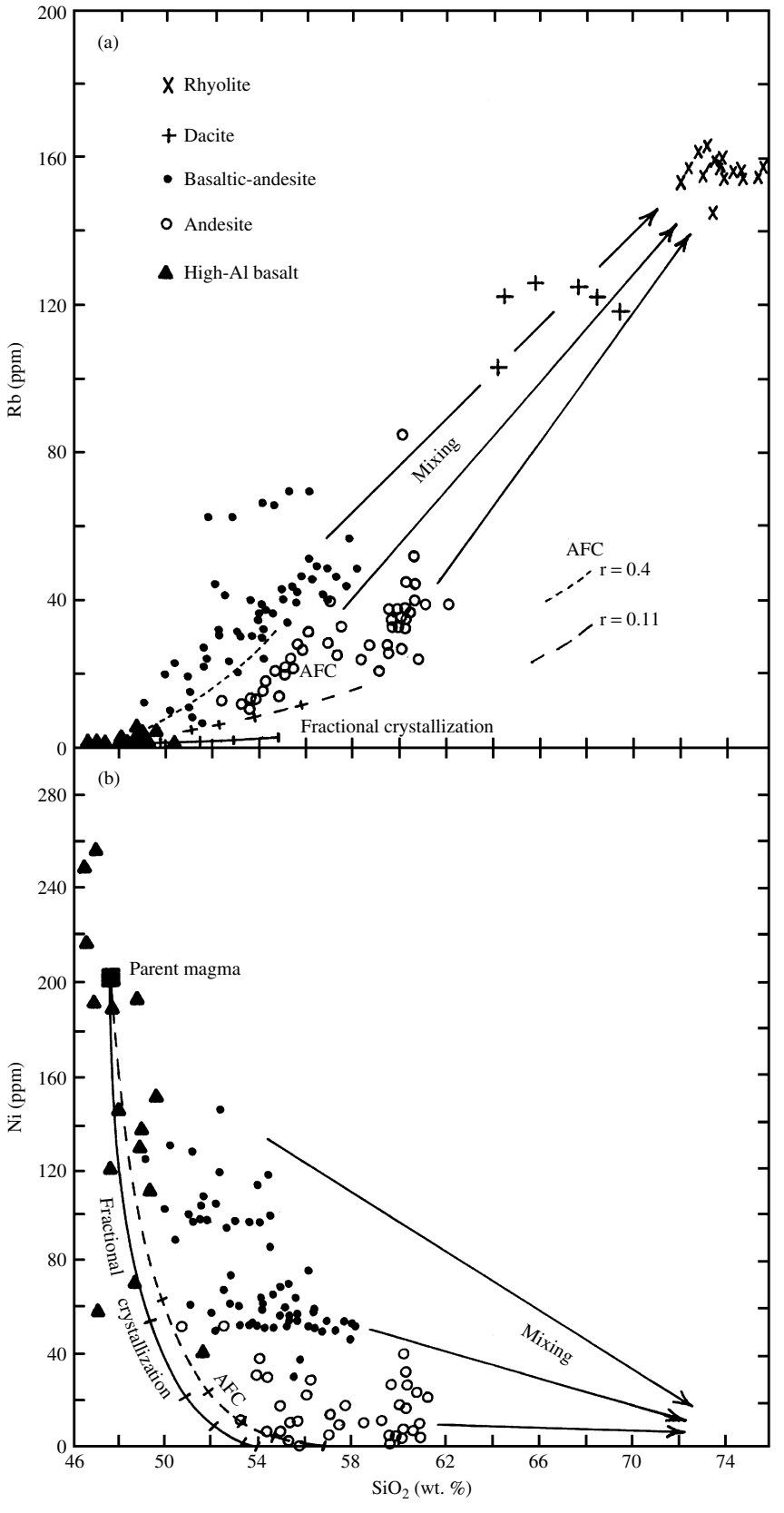


**12.29** Evolution of Quaternary lavas at Medicine Lake, northern California, by fractionation, assimilation, and mixing. Fractionation of parental high-Al basalt magma modeled by extraction of olivine + plagioclase + clinopyroxene is shown by line with tick marks at intervals of 0.1 in melt fraction to $F = 0.5$. The fractionation model accounts for the observed variations in the high-Al basalts but not other magmas that must have originated by mixing of the evolved high-Al basalt magmas with rhyolite magma together with combined assimilation and fractional crystallization (AFC). The AFC model assumes the ratio ($r$) of the rate of assimilation of feldspathic sandstone and rhyolite to the rate of fractional crystallization was 0.11 (long dashes) or 0.4 (short dashes). Fractionation involving magnetite and hornblende could not reproduce the whole suite of lavas. (Redrawn from Grove et al., 1982.)

rims. Elevated compatible element (e.g., Ni) concentrations at a particular silica content in basaltic andesites and andesites were apparently produced by mixing of high-Al basalt and rhyolite magmas (Figure 12.29b).

The remarkably similar I-type granitic rocks of the Sierra Nevada batholith in California and the Coastal batholith of Peru are plotted in $K_2O$-$Si_2O$ space in Figure 12.30a. These two plutonic calc-alkaline suites can be compared to the $K_2O$-$Si_2O$ plot in Figure 12.30b, which shows trends of residual melts resulting from fractionation of the indicated minerals from parental basalt and andesite magmas. Parent basalt magma evolves toward andesite chiefly by fractionation of olivine. Fractionation of clinopyroxene, Fe-Ti oxides, and hornblende from andesite magmas propels evolved melts along the calc-alkaline trend exhibited by the batholithic rocks in Figure 12.30a. Fractional crystallization of water-rich primitive magmas generated in the subarc mantle wedge causes residual melts to follow the calc-alkaline trend (Grove et al., 1982), in part by stabilizing hornblende, which is widely believed to be a major player in fractionating calc-alkaline magmas. Sidewall crystallization and accompanying convective melt fractionation (Figure 8.22) are probably important phenomena in production of calc-alkaline andesite-dacite-rhyolite magmas. Thick continental crust plays an important role in arresting or at least slowing mafic magmas during ascent, allowing them to fractionate.

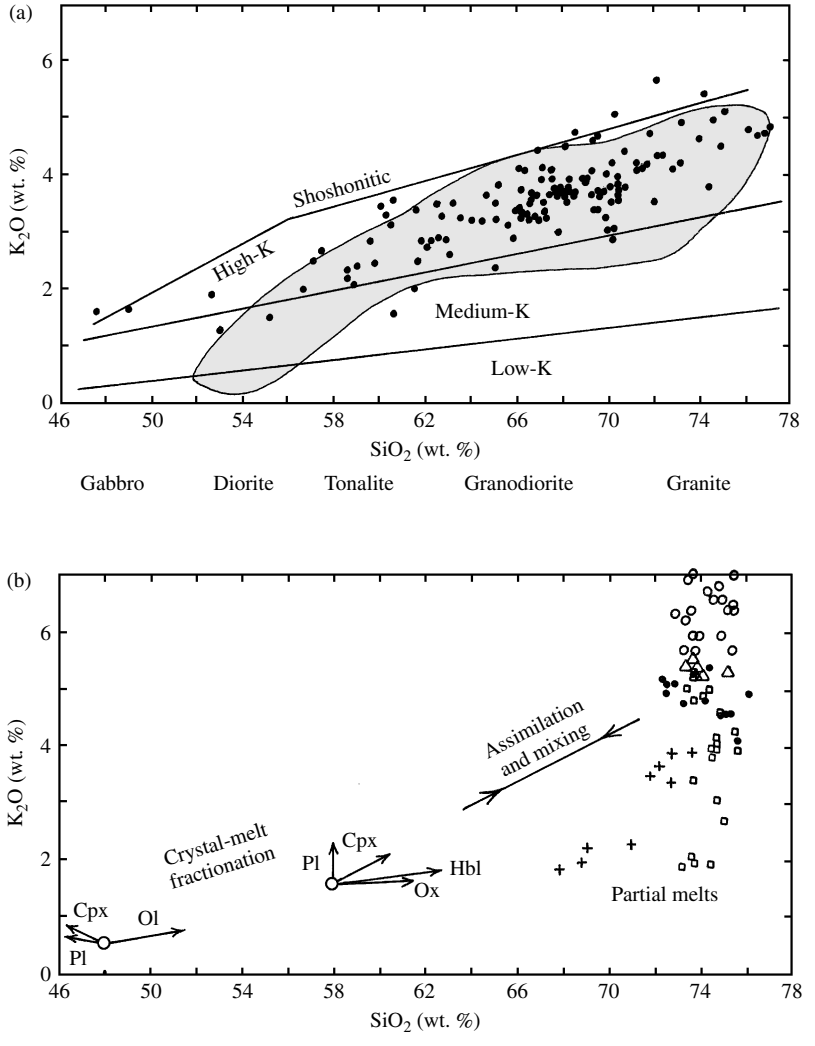


**12.30** $K_2O$-$SiO_2$ relations in calc-alkaline plutonic arc rocks. (a) Composition of rocks in the Sierra Nevada batholith, California (filled circles; from data referenced in Bateman, 1992) and in the Coastal batholith of Peru. (Shaded area from Atherton and Sanderson, 1987.) (b) On the left, trends of residual melts resulting from fractionation of indicated minerals in parental basalt and andesite magmas (open circles). On the right, compositions of experimentally generated, dehydration partial melts of pelitic source rocks (open symbols), Pl + Hbl + Qtz rock (filled circles), and feldspathic sandstone (pluses). (Data from Conrad et al., 1988; Skjerlie and Johnson, 1993; Patiño Douce and Harris, 1998; Pickering and Johnson, 1998.) Calc-alkaline batholithic rocks can be created from fractionated basaltic and andesitic parental arc magmas that are mixed with partial melts of continental source rocks.

Thick continental crust also promotes assimilation of country rock into primitive magmas. If open magma systems are contaminated by surface-derived fluids and oxidized volcanic rocks, the relatively higher $f_{O_2}$ hybrid magmas can precipitate magnetite early in their evolution, depleting residual melts in Fe and enhancing a calc-alkaline trend of silica and alkali enrichment. A high $f_{O_2}$ is consistent with the lack of a negative Eu anomaly in many continental arc rocks. On the other hand, under $f_{O_2}$, reducing conditions, generally in magma systems open only to replenishment by primitive nonarc basalt magma, such as in MORB magma chambers, the Fe-enriched tholeiitic trend develops.

Also plotted in Figure 12.30b are experimental melts generated from pelitic (clay-rich progenitors) and mafic source rocks by dehydration partial melting (Section 11.6.1). These partial melts are silicic, mostly about 75 wt.% $SiO_2$, but range widely in $K_2O$ concentration, reflecting corresponding variations in the source rock. Mixing of these partial melts with primitive as well as fractionated magmas is obviously an important process in production of calc-alkaline magmas.

Magmas developed in thick continental crust commonly have relatively radiogenic Sr and Nd isotope ratios created by contamination with ancient $^{87}Sr$-enriched rock (Figure 12.31). However, the absence of an elevated $^{87}Sr/^{86}Sr$ ratio cannot be taken as evidence for no crustal contamination because in some arcs, such as in the southern Andes, the crust is not very old and has similar isotopic composition to that of the primitive magmas. In this instance, contamination can only be discerned with trace element data or $\delta^{18}O$ values if hydrothermally altered rocks were assimilated.

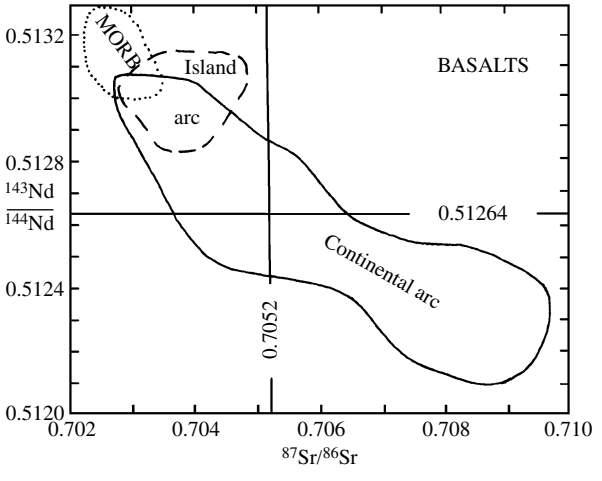


**12.31** Nd and Sr isotope ratios in arc basalts compared to MORB. Basalts from western Pacific island arcs are slightly more radiogenic than MORB because of the slab-derived aqueous fluid component, whereas continental arc basalts (Japan, Philippines, New Zealand, Ecuador, Central America, Lesser Antilles) range to much more radiogenic ratios because of interaction with highly radiogenic old continental crust in which $^{143}Nd/^{144}Nd$ can be 0.510 and $^{87}Sr/^{86}Sr$ 0.900. (Redrawn from Tatsumi and Eggins, 1995.)

## SUMMARY

A wide spectrum of magma-generating conditions in compositionally variable sources compounded with a wide range of differentiation overprints account for the wide spectrum of magmatic rock compositions found on Earth (e.g. Figure 2.4).

Despite their treatment in separate chapters, magma generation and differentiation in natural systems may be a continuum of processes, acting sequentially or possibly, to some degree, simultaneously. For example, it is reasonable to believe that, as basaltic melts segregate and begin to ascend buoyantly out of their mantle source, some precipitation of olivine might immediately occur during initial decompression and cooling. Or, as felsic magma is generated in the lower continental crust, it may simultaneously mix with basaltic magma that is providing heat for partial melting; assimilation of wall rock may also concurrently occur. To understand the origin of magmas, the petrologist must sort out signatures related to primary generation versus secondary differentiation in suites of comagmatic rocks, using their mineralogical, elemental, and isotopic compositions as well as their fabric and field relations.

Few magmas are likely to rise very far from their source without overprinting modifications in composition. Overprinting processes include closed-system differentiation—chiefly crystal-melt fractionation—and open-system mixing of magmas and assimilation of country rock. Crystal-melt fractionation by crystal settling, filter pressing, and convective melt fractionation is important in the differentiation of tholeiitic magmas emplaced in continental and oceanic crust, producing a trend of Fe enrichment with limited felsic differentiates. These basaltic intrusions may be open to replenishment by more draughts of primitive magma that mix with the crystallizing magma. In MORB chambers this replenishment and mixing apparently occur so frequently that modification of magma composition is limited; consequently, most MORB constituting the floor of the oceans is relatively uniform tholeiitic basalt.

Mantle-derived basaltic magmas can underplate or stall within the lower continental crust, cool, fractionally crystallize, and give off latent heat to allow assimilation of country rock (AFC). Mixing of mafic and more silicic magmas also occurs. Altogether, these processes produce calc-alkaline rock suites typical of continental margin magmatic arcs. The fractional crystallization ac-

companying assimilation is particularly effective in producing the calc-alkaline trend if it occurs under elevated water and oxygen fugacities. Thicker continental crusts allow more opportunity for AFC and mixing, so that in thickest crusts, as in the central Andes of South America, little, if any, primitive mantle-derived basaltic magma is extruded and most shallow intrusions and extrusions are of rhyolite, dacite, and andesite.

## CRITICAL THINKING QUESTIONS

12.1 Essentially monomineralic layers of pyroxenite, dunite, or anorthosite in large differentiated basaltic intrusions can only form by crystal accumulation because no magmas of equivalent composition are known to occur. What do you think is the evidence for no such magmas? (*Hint:* Consider the volcanic record.)

12.2 How do monomineralic layers (see preceding question) originate? Even the least "porous" cumulate still has a significant proportion of interstitial basaltic melt entrapped between the cumulus crystals.

12.3 Why are Sr and Nd isotopic ratios *not* used to evaluate details of crystal-melt fractionation in magma systems?

12.4 Explain the origin of the seven textural types of olivine grains in the 1959 summit eruption of Kilauea, Hawaii (Special Interest Box 12.1). Which are mantle-derived, cumulates, or precipitates of ascending magma?

12.5 Mixed magmas erupted from volcanoes can have an essentially homogeneous melt, but crystals are commonly markedly inhomogeneous and display disequilibrium textures and locally complex zoning. Why?

12.6 Why is assimilation probably insignificant in the evolution of MORB magmas crystallizing in oceanic crustal magma chambers?

12.7 Critically evaluate the origin of pegmatites, especially their distinctive fabric, in terms of the Jahns-Burnham model involving volatile-oversaturated magma systems versus the London model involving kinetic factors in an undercooled magma system.

12.8 Contrast primary, primitive, and parent magma—their differences and ways each can be discerned.

12.9 (a) Does the immiscible Fe-rich glass in mesostases of some tholeiitic basalts (column 1, Table 12.3) resemble any common silicate rock? (b) In what ways does it differ from other rocks of comparable silica content?

12.10 Examine Figures 12.30, 2.18, and 13.24. Is contamination of mantle-derived basaltic magmas with continental crust a viable means of creating highly potassic magmas that form the shoshonite series? Discuss.

12.11 What are the different ways that andesitic magmas can be produced in arcs? What trace element and isotopic attributes would distinguish among these?

12.12 Rocks originating by mingling of two magmas and by physical separation of immiscible melts may be superficially similar. What rock attributes would distinguish between these origins?

## PROBLEMS

12.1 Evaluate the validity of hornblende fractionation from a parental andesite magma in producing rhyolite and dacite daughter magmas. Use compositions from Table 2.2 and Appendix A on two-element variation diagrams. Critically discuss your results.

12.2 In Figure 12.29a, what was the approximate proportion of rhyolite magma that mixed with andesite magma that contains 60 wt.% $SiO_2$ to create dacite that contains 69.5 wt.% $SiO_2$?

12.3 Write a stoichiometrically balanced reaction for assimilation of Al-rich minerals and rocks by basalt magma to yield anorthite and enstatite components in the hybrid contaminated magma at the expense of diopside in the basalt. Use $Al_2SiO_5$ to represent the aluminous material. What bearing might this assimilation have on the origin of some leuconorite?

12.4 Write balanced mineralogical reactions showing how: (a) An initially subalkaline, silica-saturated magma that contains normative enstatite and orthoclase could become silica-undersaturated with normative diopside and leucite by assimilating limestone. (b) Silica from the magma can metasomatize wall rock and xenolithic limestone and dolomite, producing calcium silicate minerals such as wollastonite and diopside. Discuss how effective these reactions are in modifying the degree of silica saturation in the original magma.

12.5 Examine the consequences of assimilation of crystalline material into magma using the binary system $NaAlSi_3O_8$-$CaAl_2Si_2O_8$ as a model. Consider a model magma that contains crystals of plagioclase $An_{40}$ in equilibrium with melt into which crystals of cool $An_{60}$ and of $An_{20}$ are introduced. Compare and contrast the subsequent evolution of the two magmas as they crystallize.

12.6 Le Roex et al. (1990) show that the basanite-phonotephrite-tephriphonolite-phonolite sequence on Tristan da Cunha (Figure 2.16) was created by crystal-melt fractionation. This

**Table 12.7.** Concentrations of $SiO_2$, Rb, and Sc and Distribution Coefficients for Rb and Sc in Tristan da Cunha Lavas

| | Basanite | | | | | | | | | | Phonotephrite | | | | | | | Tephriphonolite | | | | | Phonolite | | |
|---|---|---|---|---|---|---|---|---|---|---|---|---|---|---|---|---|---|---|---|---|---|---|---|---|---|
| | SP | A | A | A | A | SP | SP | A | SP | A | P | A | A | A | P | P | P | A | P | P | A | A | SP | SP | P |
| $SiO_2$ | 44 | 45 | 44 | 46 | 46 | 46 | 44 | 46 | 44 | 46 | 50 | 48 | 48 | 51 | 50 | 48 | 48 | 55 | 57 | 56 | 55 | 55 | 61 | 58 | 59 |
| Rb | 73 | 64 | 62 | 75 | 73 | 78 | 74 | 71 | 65 | 76 | 112 | 90 | 80 | 95 | 119 | 88 | 87 | 129 | 151 | 153 | 139 | 128 | 176 | 151 | 165 |
| Sc | 18.1 | 17.1 | 22 | 14.5 | 14.7 | 13.9 | 17 | 12.7 | 14.6 | 10.3 | 4.4 | 10.1 | 9.3 | 6.2 | 5.4 | 6.5 | 7.8 | 3.1 | 2.7 | 2.6 | 2.5 | 3.4 | 1.3 | 1.6 | 1.3 |

| | Cpx | TiMag | Pl | Amph | Alk feld |
|---|---|---|---|---|---|
| Rb | 0.01 | 0.01 | 0.01 | 0.5 | 0.6 |
| Sc | 4 | 20 | 0.01 | 4 | 0.01 |

$SiO_2$ concentrations rounded to nearest whole number weight percentage; Rb and Sc, parts per million; A, aphyric; P, porphyritic; SP, sparsely porphyritic.
(From Le Roex et al., 1990.)

fractionation can be approximated by considering just two trace elements—Rb and Sc. (a) Are these elements compatible? Incompatible? (b) Using the data in Table 12.7, make a plot of Rb versus Sc for the sequence of rocks. (c) Which sample would be a reasonable parent magma for the sequence? (d) Determine bulk distribution coefficients for Rb and Sc that, when used in equation 12.1, yield a model Rb-Sc curve fitting the data points as closely as possible. Can the entire sequence be modeled by one set of coefficients? Discuss. (e) What weight proportions of clinopyroxene (Cpx), titaniferous magnetite (Ti-Mag), and plagioclase (Pl) account for differentiation of the basanite-phonotephrite part of the sequence? Discuss your results. (f) Can the tephriphonolite-phonolite suite be produced by fractionating the same minerals? Others? Discuss.

12.7 If the immiscible Fe-rich glass in column 1, Table 12.3, were to crystallize, of what minerals would it be composed and what would be their modal proportions? Assume an oxygen fugacity buffered by QFM (Figure 3.14).

12.8 For the shonkinite-syenite association in Table 12.3 plot the first 13 trace elements listed on a primitive-mantle normalized diagram (Table 2.7). How do the two patterns compare with those for other rocks in this textbook? Is it possible that these two rocks could be related by fractional cystallization, rather than by separation of immiscible melts? Critically evaluate whether fractionation of common rock-forming minerals might account for the trace element contents of the two rocks. For example, are the Co and Ni contents consistent with olivine fractionation? Ti and V with Fe-Ti oxide fractionation? And so on.